Pergamon

Journal of Structural Geology, Vol. 16, No. 6, pp. 795 to 815, 1994

0191-8141/94 $07.00+0.00

Microfracturing, paleostress and the growth of faults

MARK H. ANDERS

Department of Geological Sciences and Lamont-Doherty Earth Observatory, Columbia University, Palisades, NY 10964, U.S.A

and

DAVID V. WILTSCHKO

Center for Tectonophysics and Department of Geology, Texas A&M University, College Station, TX 77843, U.S.A.

(*Received* 15 *October* 1992; *accepted in revised form* 5 *July* 1993)

Abstract—We have analyzed the microfractures in samples taken near one thrust fault and five normal faults of known displacement to test the dependence of microfracture density and distribution on fault slip. We have also recorded the orientation of microfractures as a function of distance from the associated fault surface. In order to control as many parameters as possible, shallow faults with similar lithologies were chosen. They showed the same kind of deformation, namely, microfracturing without block rotation, recrystallization, extensive granulation or crystal plasticity. The results of over 8000 microfracture measurements suggest that maximum microfracture density is independent of net slip. We interpret this relationship as indicating that the preponderance of microfracturing occurs in proximity to the propagating fault tip. The angular relationship between the shear plane and microfractures was commonly found to be between 5° and 20°, significantly less than the ~30° expected between the far-field maximum principal stress and the shear surface. This low angle between microfracture orientation and shear plane orientation is predicted for a local stress field associated with a propagating mode II fault tip. Other possible explanations for the small angle for tensional microfractures and the shear surface are: (1) the effective confining pressure was very low; or (2) shear strength at failure was much larger than expected.

INTRODUCTION

EXPERIMENTS on various rock types as well as model and field studies indicate that microfractures are both good indicators of the orientation of the principal stresses and important precursors to the formation of a through-going slip surface (e.g. Tuttle 1949, Borg *et al.* 1960, Friedman 1963, Brace & Bombolakis 1963, Scholz 1968, Dunn *et al.* 1973, Hallbauer *et al.* 1973, Sangha *et al.* 1974, Engelder 1974, Friedman *et al.* 1976, Tapponnier & Brace 1976, Brock & Engelder 1977, Knipe & White 1979, Lespinasse & Pecher 1986, Kowallis *et al.* 1987, Laubach 1988, 1989). These studies show that microfractures form long-axis parallel to externally applied σ_1 and short-axis parallel to the externally applied σ_3. Microfractures may occur within grains, along grain boundaries or be continuous through two or more grains (see Kranz 1983). Experimental studies show that with increased stress, microfracture activity begins to concentrate along the eventual fault surface and previously formed microfractures obliquely link up to produce a slip surface at some angle to σ_1 (Scholz 1968, Brace 1971, Hoshino 1972, Dunn *et al.* 1973, Hallbauer *et al.* 1973, Friedman 1975, Friedman *et al.* 1976, Lockner *et al.* 1991). Microfractures are thus both indicators of the stresses which cause faulting as well as participants in that process.

Several workers (Friedman 1969, Engelder 1974, Brock & Engelder 1977, Knipe & White 1979, Kanaori *et al.* 1991) have examined microfracturing near natural faults and found that microfracture density increases as a fault contact is approached. Brock & Engelder (1977) describe microfractures as an early manifestation of faulting, and noted that the number of microfractures produced is markedly retarded everywhere except near the fault during the generation of fault gouge. Macrofractures also have been used to assess the orientation of the stress field around naturally occurring faults (see Hancock 1985). In a similar manner to microfracturing, macrofracture density has also been shown to decrease as a function of distance from respective fault planes (Brock & Engelder 1977, Chernyshev & Dearman 1991).

We report here on an investigation of the relationship between brittle faulting and cataclasis of the surrounding rock in the absence of rotation, granulation, recrystallization or evidence of plastic flow. We have selected faults of measurable displacement which affected similar lithologies at shallow depth in order to control variables other than fault slip. Our results show that the effect of displacement on microfracture density is small to non-existent for the rocks studied and that the σ_1 directions indicated by our microfracture concentration data are significantly closer to the shear surface than the 30° that we expected based on many of the above mentioned studies.

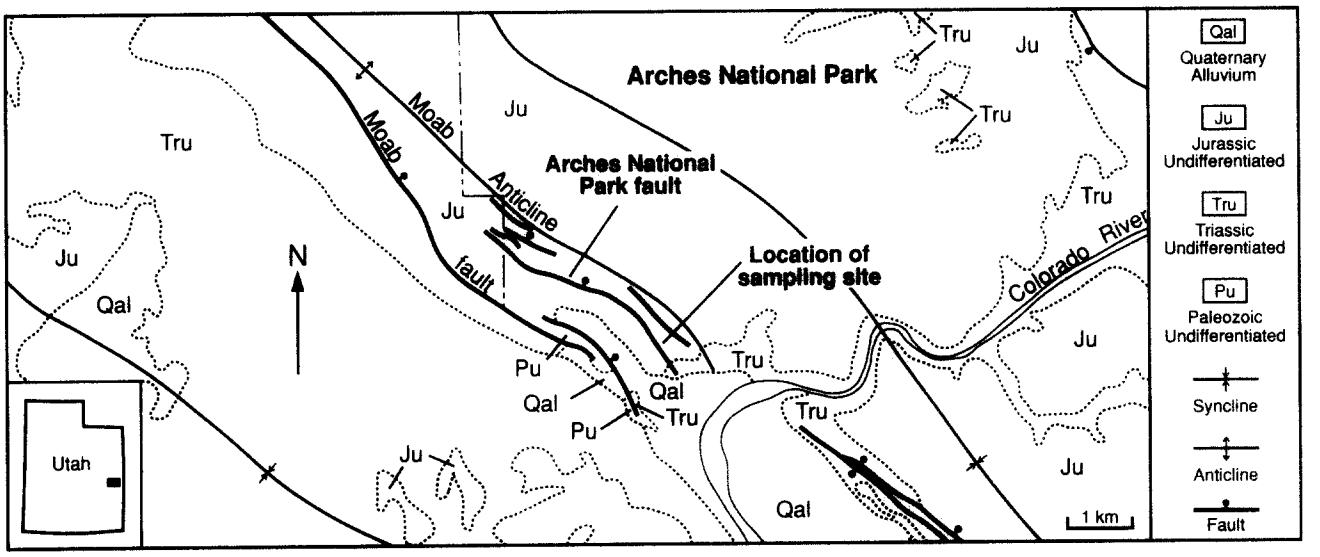

Fig. 1. Generalized geologic Map of Arches National Park. Modified from Baker (1933) and Cater (1970).

GEOLOGIC AND GEOGRAPHIC SETTING

Arches National Park

One of the normal faults selected for study is on the southwest flank of the Moab anticline near the entrance to Arches National Park (Fig. 1). Baker (1933) describes the Moab Valley anticline as a salt anticline similar in structure and genesis to other anticlines of the Paradox Basin. In his view, normal faults paralleling the anticlinal axes are the result of salt removal from the Paradox member of the Hermosa Formation, and subsequent collapse of overlying rock.

Depth of faulting is estimated by Cater (1970, p. 65) to be about 1.7 km for anticlinal valleys of the Paradox Basin. This compares with a depth of 1.8 km we calculated for the Arches National Park fault, in part based on the Moab area stratigraphic column provided by Baker (1933).

The fault that we have sampled is in a sequence of Jurassic fine-grained Eolian sandstones and its orientation was described by Lohman (1975, p. 61) as vertical although our measurements indicate that the fault dips about 54°N ± 10°. The fault surface is not perfectly planar, but rather gradually decreases in dip downward. Our strike measurements were found to be within 10° of the strike of the Moab anticline (Fig. 1). Net slip was calculated to be 67 m ± 5 m based on slickenside data and apparent displacement measurements.

The fault surface and the rock volume immediately surrounding it exhibit little evidence of deformation or extensive gouge. There are, however, planar zones of deformation bands a few millimeters thick paralleling the fault. Aydin & Johnson (1978) describe similar features at Arches National Park, in which the sand grains are crushed. The deformation bands are generally parallel to the fault surface and occur at distances as much as 2 m away, although many of the deformation bands at Arches National Park are not restricted to a particular fault zone (see Aydin 1978, Aydin & Johnson 1978). The deformation bands located away from the fault seldom exhibit visible displacement. No evidence of block rotation or gradation in rock texture is observed as a function of distance from the fault. The fault is sharp and well exposed. It splays into parallel minor faults and horsetails only at the most distal exposure of the fault.

Flagstaff Mountain

Boulder fault, a 'Laramide age' thrust fault, was sampled on Flagstaff Mountain southwest of Boulder, Colorado (Fig. 2). The exact age of faulting is difficult to assess because the youngest offset unit is the late Cretaceous Pierre Shale and the oldest undisturbed unit is the early Quaternary Rocky Flats Alluvium. This thrust dips 34° to the west and thrusts late Paleozoic rock over late Mesozoic along the eastern flank of the Front Range. Maximum displacement was determined to be 1.5 km at Flagstaff Mountain based on stratigraphic omission. The fault length is difficult to assess because the fault surface is untraceable in the Cretaceous shale north and south of the sampling site. Depth at this location at the time of faulting is estimated to be less than 3.5 km based on the thickness of the stratigraphic section in the Denver Basin to the east of the Front Range. Two rock types were sampled, the Lyons Sandstone and the Fountain Formation. The Lyons Sandstone is the most intensely deformed. The Lyons Sandstone exhibits both extensive small slickensided faults roughly parallel to the main fault contact as well as numerous oblique fault splays. Some samples of Lyons Sandstone exhibit cataclastic zones that are so fine grained that they are extinct under cross nicols. However, these are only a few millimeters thick and make up only a small percentage of the rocks sampled.

Drotar Ranch

The Drotar Ranch fault is a complex of small normal faults located in the southern part of Larimer County, Colorado (Fig. 3). An oblique view of this fault is seen in

the upper left-hand corner of fig. 10 in Matthews & Work (1978). The major branch (labeled 'B' in Fig. 4) has a net slip of 6 m, and the two smaller splay faults (labeled 'A' and 'C', Fig. 4) have net slips of 1 and 2 m, respectively. The depth of burial at the time of faulting is also estimated to be less than 3.5 km based on the pre-Tertiary thickness of sediments in the Denver Basin.

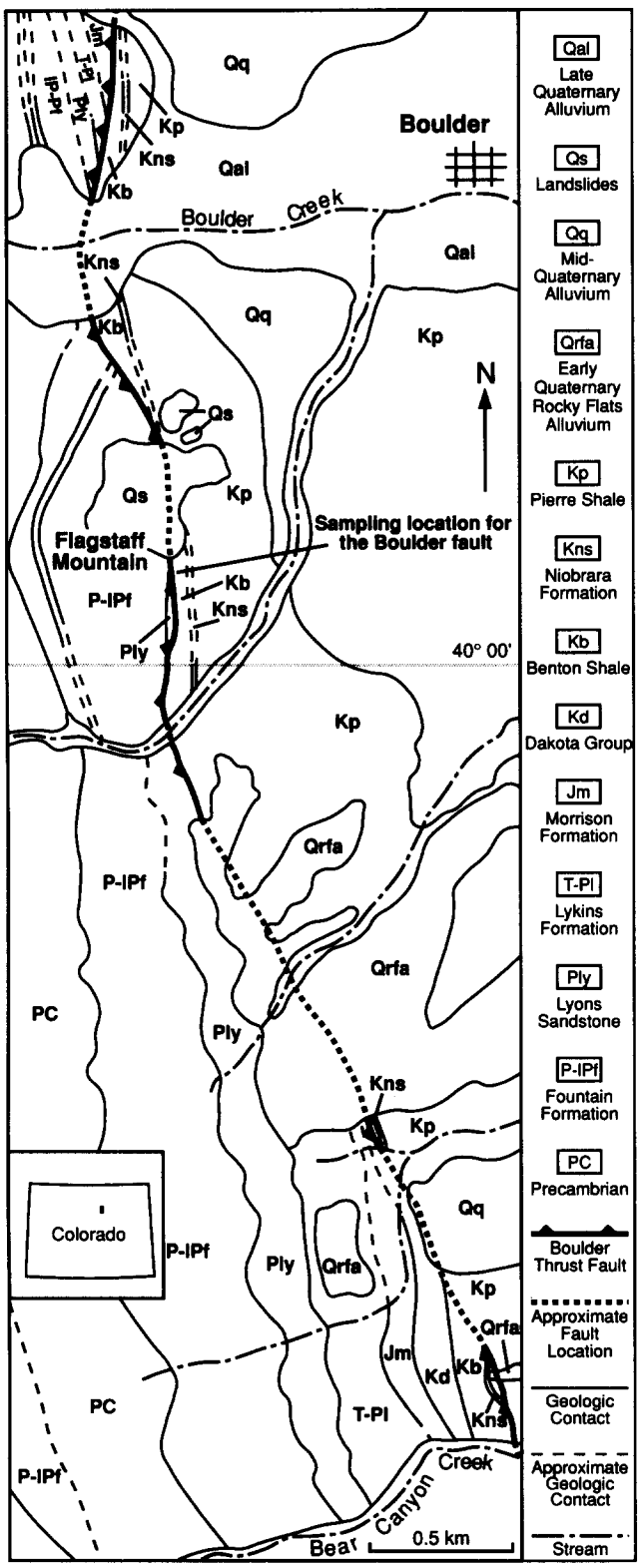

Fig. 2. Generalized geologic map of the area surrounding the Boulder fault sampling location.

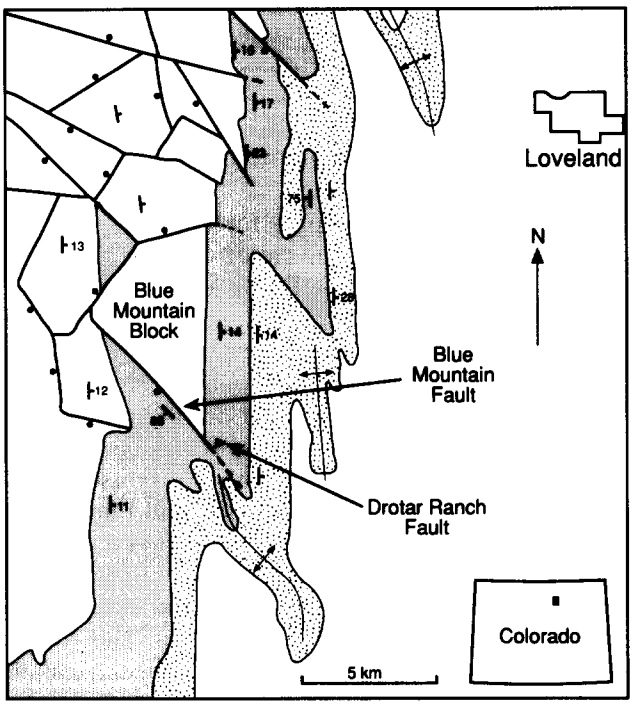

Fig. 3. Generalized geologic map of the area surrounding the Drotar Ranch fault sampling location. Dark stippling is for Paleozoic rocks and the light stippling is for Mesozoic rocks. Modified from Matthews & Work (1978).

Matthews & Work (1978) suggest that Blue Mountain, the topographic feature on which the Drotar Ranch fault is located, is formed by readjustments of a discrete crustal block along deep vertical faults of Laramide age. Matthews & Work (1978) further suggest that the valley in which Drotar Ranch is located was deformed into a graben by a similar crustal-block readjustment. The large normal fault bounding the southern escarpment of Blue Mountain (Fig. 3) we will refer to as the 'Blue Mountain fault'. The Drotar Ranch fault is located about 100 m from the Blue Mountain fault near its southeasternmost tip where we estimate about 30 m of offset. As with the Boulder thrust fault, the exact age of movement is difficult to assess because the oldest

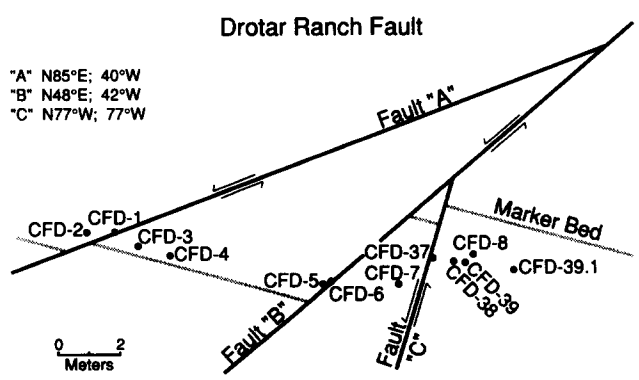

Fig. 4. View looking northward toward three small normal faults in the Fountain Formation along the southwest escarpment of Blue Mountain at Drotar Ranch. Diagram is normal to the strike of fault 'B'. Faults 'A' and 'C' are traces on a vertical plane oriented N42°W. Because of high calcite content samples 1, 6, 7 and 8 were not assessed for microfracture orientation or density. See Fig. 3 for location of fault.

undisturbed rocks are Quaternary and the youngest offset rocks are late Cretaceous.

LITHOLOGY

The geologic units sampled for this study are the Entrada, Navajo and Lyons sandstones and the Fountain Formation arkose. The Entrada and Navajo sandstones are sampled in Arches National Park and the Lyon Sandstone and Fountain Formation are from the Drotar Ranch and Flagstaff Mountain sites located along the eastern Front Range of north central Colorado. The Upper Jurassic Entrada Sandstone and the Lower Jurassic Navajo Sandstone are cross-bedded, fine-grained sandstones of probable sand dune origin (Lohman 1975). We found grains in both of these units to be well rounded and uniform in size averaging about 0.15 mm; calcite is the most common cement although clay and hematite cement are common. The Navajo Sandstone that we sampled has a larger calcite content and lower hematite content than the Entrada Sandstone although the sum of the modes of calcite and hematite are the same for both sandstones. Average porosity values are 24 and 25% for the Navajo and Entrada Sandstone, respectively. Both sandstones that we sampled were friable although the Navajo Sandstone at other locations has been described as well cemented (Aydin 1978). The Carmel Formation, which separates the Navajo and Entrada sandstones, was sampled but microfractures were too rare to be statistically significant. The lack of microfractures is due to the reduced sand fraction which limits the number of grain-to-grain contacts.

The Pennsylvanian–Permian Lyons Sandstone also is a cross-bedded fine-to-medium-grained sandstone, also thought to be a dune deposit (Hubert 1960). The Lyons Sandstone is largely cemented by silica, and we found the average porosity to be about 5%.

The Fountain Formation is a Pennsylvanian arkose consisting of angular to subangular, medium to clast-sized quartz and feldspar grains. The depositional environment is described to be one of accumulating alluvium off the flanks of the ancestral Rocky Mountains (Hubert 1960). The sum of the calcite plus hematite fraction is approximately 30%, the dominant cementing agent is calcite (Table 1). Porosity is variable with an average for all Fountain Formation samples of about 9%.

SAMPLING TECHNIQUE

Faults were selected based on the access to the fault plane, the ability to constrain the orientation of the fault plane, and the ability to make good estimates of net slip. Oriented samples were taken at various distances up to 500 m in a direction normal to the fault surfaces on both the hanging wall and footwall. Sample distance from the faults were either measured with measuring tapes or surveyed. Net slip for all faults was determined trigonometrically, using the orientation of the fault surface, slickensides and measurable displacements of geologic features observed along fault contacts. Fault plane orientations were measured directly except in the case of the Boulder fault surface at Flagstaff Mountain, which was determined by several three-point-problem solutions. Due to the quality of the fault surface exposure, the sampling distance for Boulder fault should be considered less accurate than for other faults sampled. Sampling closer than 3 m on the Boulder fault was not done because of possible block rotations directly adjacent to the fault surface.

Samples collected in the field were coated with epoxy and then three thin sections were cut such that each section corresponded to one of three mutually perpendicular directions related to the surface containing a strike-dip marker. For samples within a few centimeters of the fault the marker surface was the fault plane. Resulting microfracture measurements were rotated into a common viewing direction related to the shear surface and slip direction of their respective faults.

MICROFRACTURE MEASUREMENT TECHNIQUE

Borg *et al.* (1960, p. 169) noted that microfractures with orientations greater than 45° from the viewing direction are not detectable with a universal stage microscope and that there is a strong preference for measuring fractures that are oriented 20° from the viewing direction. We have, therefore, taken extra care to make maximum angular sweeps from the vertical down to a 45° dip in all three sections. A concerted effort was made especially to look for and measure microfractures that are close to the 40–45° limit of detectability. Lack of care in this aspect results in equal-area stereonet plots with a characteristic pattern of two perpendicular vertical girdles and one horizontal girdle all exhibiting a roughly 20° scatter (e.g. Dula 1981, his fig. 5, Row B, samples DNC-2, DC-7 and DC-9). This operator bias arises because fractures oriented less than 20° from the vertical are most easily seen and measured. By looking for microfractures oriented more than 20° away from vertical, we may still have some 'blind' spots but their size is greatly reduced.

Some of our data appear to have two of the three operator bias girdles. However, we are confident that these are not an artifact, based on the following argument. All thin sections were cut in orientations related to available flat surfaces where the best measurement of strike and dip could be made; the data were rotated into a single orientation with reference to the fault slip. Because the fault slip and fault surface directions are not the same, a girdle of pole plot points induced by operator error should *not* be along the perimeter and/or 90° to it. However, most of the girdles of pole plot points do so, which suggests that these concentrations are not statistical aberrations.

Another potential problem in interpreting microfracture data is the effect of preferential fracturing in some crystallographic orientations. Rowland (1946) and Borg & Maxwell (1956) found that quartz grains in both sand and sandstones were dominantly elongate parallel to the *c*-axis. In addition, Borg & Maxwell (1956) and Borg *et al.* (1960) found that there was a preferred orientation of fractures in quartz grains along $r\{1011\}$ and $z\{0111\}$ surfaces, even though other fracture orientations were observed. While Borg & Maxwell (1956) and Borg *et al.* (1960) differ as to the importance of the other crystallographically controlled fracture planes, both agree that $r\{1011\}$ and $z\{0111\}$ are by far the most important. Borg & Maxwell (1956, p. 80) further agree that this preferred orientation of fracturing is so weak that the effect on their results is insignificant. Quartz grains, to a good first approximation, act as an isotropic medium in which the microfractures propagate.

The last effect that must be evaluated is sample size. It is clearly important to select the number of measurements that best represent the net orientation of microfracturing. Due to the inhomogeneity of the interaction between the stress field and rock at the grain scale, and the likelihood of inherited microfractures, any given microfracture in itself may not represent the gross stress field.

It is important to determine the maximum number of microfractures that accurately determine the mean fracture orientation yet minimize time. To solve this problem other authors have used numbers of measurements ranging from around 100 to 300 fractures (e.g. Engelder 1974, Brock & Engelder 1977, Borg *et al.* 1960, Friedman 1963). Others used more; Borg *et al.* (1960) and Halbauer *et al.* (1973), made 919 and 648 measurements, respectively. With the exception of Simmons *et al.* (1975), who attempted to correlate microfractures with elastic properties of rock, there have been no efforts to determine the number of microfractures that accurately define a statistical fabric orientation within acceptable statistically determined limits.

To evaluate the role of sample size, all of our data for one site, Arches National Park, were combined into one data set and then randomly sampled in multiples of 25 microfracture orientations. For each population from 25

Table 1. Microfracture density, mineralogy and distance from fault plane

Sample	Unit sampled	Location	Microfracture density*	Distance from fault plane†	Mineralogy (percent)			
					Quartz	Feldspars	Calcite	Hematite
CFD-1			102.5	0.02	60	8	30	1
CFD-2			78.8	0.40	50	5	28	15
CFD-3			55.8	0.60	58	12	24	2
CFD-4			66.5	1.2	59	10	28	2
CFD-5	Fountain Formation	Drotar Ranch	77.6	0.15	63	10	24	2
CFD-37			88.0	0.03	57	9	28	5
CFD-38			52.2	0.80	59	6	23	11
CFD-39			40.4	1.20	60	9	23	7
CFD-39.1			48.3	2.75	57	14	20	7
CLD-51				0.23	70	1	22	
CLD-52	Lyons Sandstone	Drotar Ranch		0.46	78	1	13	8
CLD-53				1.22	60	1	23	16
CLD-54				4.57	55	2	27	16
UNA-33			7.1	0.02	74	2	23	1
UNA-35			3.7	1.22	55	2	41	1
UNA-37	Navajo Sandstone	Arches National Park	3.4	0.02	76	0	22	2
UNA-38			3.5	0.30	63	1	26	10
UNA-39			4.5	0.60	57	3	34	6
UNA-42			3.6	3.00	53	2	44	1
UNA-70			1.29	18				
UNA-71			1.25	485				
UEA-23			4.8	0.15	65	3	17	15
UEA-24			4.6	0.30	62	4	17	18
UEA-27			2.2	1.07	61	3	17	17
UEA-34	Entrada Sandstone	Arches National Park	8.8	0.03	71	5	19	5
UEA-36			4.0	0.20	65	2	25	8
UEA-40			4.3	1.20	54	2	19	4
UEA-41			3.5	0.60	53	3	26	17
UEA-60			1.1	57				
UEA-61			1.8	200				
CFF-1			25.0	3	59	14	21	5
CFF-2			33.75	5	55	10	19	15
CFF-3	Fountain Formation	Flagstaff Mountain	17.6	7	67	12	9	11
CFF-4			21.2	20	64	12	18	14
CFF-5			12.3	35	54	8	17	16
CFF-6			5.4	101				
CFF-7			6.9	128				
CFF-8			5.4	244				
CFF-9			6.8	437				

*Number of fractures that intersect a random 1 mm line (average of 25 lines).
†In meters, the Boulder fault could not be located to the accuracy of other faults.

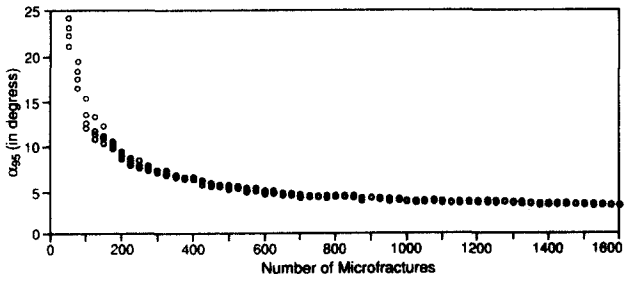

Fig. 5. Plot of α_{95} vs number of microfractures. Four program runs were made using increments of 25 randomly selected microfractures out of a total data file of 1600 microfractures.

to 1600, a statistical test for the cone of confidence of the mean direction was made (Fig. 5). The α_{95} values show that for samples greater than about 600, the cone of confidence is 5°. For a sample size of 100–200, the cone of confidence is 2–3 times greater than for 600 samples. For this study we have used plots ranging from 100 to about 300 microfractures for individual sites and up to 2552 for combined sites. The smaller sample size is most likely toward the lower end of what is statistically defensible. For a single sample, one would expect a more homogeneous population of microfractures and therefore fewer would be necessary to characterize it. The number of microfractures necessary to define a statistically significant population will vary significantly as a function of both rock type and the relative contribution of inherited microfractures. Rock samples in which crystals intergrow or are cemented by quartz will require fewer measurements than rocks like the Fountain Formation sandstones that are poorly cemented, resulting in stress concentrations at grain–grain contact points. Nevertheless, a sample size evaluation should be made based on reproducibility, geologic significance and the conformity to reasoned expectations (M. Friedman personal communication, 1992).

Character of microfracturing

There are two general types of fractures in the rocks studied: (1) straight fractures that cross multiple grain boundaries; and (2) fractures that traverse only a single grain. Both types of microfractures exhibit aspect ratios on the order of 10^{-4} and are recognizable by the alignment of 'bubbles' which are either fluid inclusions or mineral precipitates deposited when the microfractures were open to pore fluids. The name 'healed microfractures' is often given to microfractures exhibiting these characteristics. The straight fractures that cross multiple grain boundaries generally occur in well cemented, low porosity samples. Quartz rims presumably caused the sandstone to act as a homogeneous unit through which the fracture would travel (Gallagher *et al.* 1974). This type of fracture, as represented in sample CLD-53 (Figs. 6a & b), is rare in all but the Lyons Sandstone, the lowest porosity rock we studied.

The second type of fracture was prevalent in almost all samples. These fractures are distinguished by their curvilinear shape (Figs. 7a & b), and their tendency to radiate from distinct locations on the grain boundaries. These fractures are thought to emanate from, and radiate to, locations where individual quartz grains contact each other (see Gallagher *et al.* 1974, Gallagher 1987, Lloyd & Knipe 1992). In rock with this type of fracturing, quartz overgrowths are rare and microfractures are not traceable across grain boundaries. Microfractures restricted to one grain also leave open the possibility of any given microfracture we measure being inherited. We have tested for this possibility by sampling microfracture orientation and density at increasing distance from the fault surface in order to establish a background level of microfracturing.

In thin sections exhibiting the second type of fracturing, we found it extremely rare to observe a grain contact location with radiating fractures. This is due to the small probability of such a contact occurring in a 30 μm slice of a 2 mm quartz grain that has an average of only 12 grain-contact points. Although the points of contact are not visible on most grains, fractures radiating away from these points of contact are pervasive throughout the grain and are observable on all possible cross-sections as a distinctive *en échelon* curvilinear pattern. Again, these patterns are ubiquitous in samples where quartz overgrowths are not present.

Based on observations of tens of thousands of microfractures in our study, no microfractures were seen to offset grain boundaries or offset any other features observable within quartz grains, i.e. shear displacement along these microfractures is negligible. From these observations we conclude that the microfractures are tensional mode I fractures and can be used to assess the local stress field.

RESULTS

Microfracture density

Microfracture density is one of the most reliable measures of cataclasis and as such is used by numerous authors to record the intensity of deformation. Values for whole rock microfracture density can be obtained from measurements of thin sections (Borg *et al.* 1960, Simmons *et al.* 1975). Therefore, in our study, microfracture density is derived by counting the number of microfracture traces that intersect a 1 mm long line. On each of the three mutually perpendicular thin sections from 10 to 25 random locations are selected for counting. For each sampling site, the number of fracture intersections along the count lines is measured on the three mutually perpendicular thin sections and is divided by the number of counts. This yields microfracture density in terms of the number of microfracture intercepts per millimeter (referred to as linear intercepts mm^{-1} or microfractures mm^{-1}). It is difficult to compare the microfracture density from one study to another. This is because microfractures are most visible when viewed on-end and invisible when viewed normal

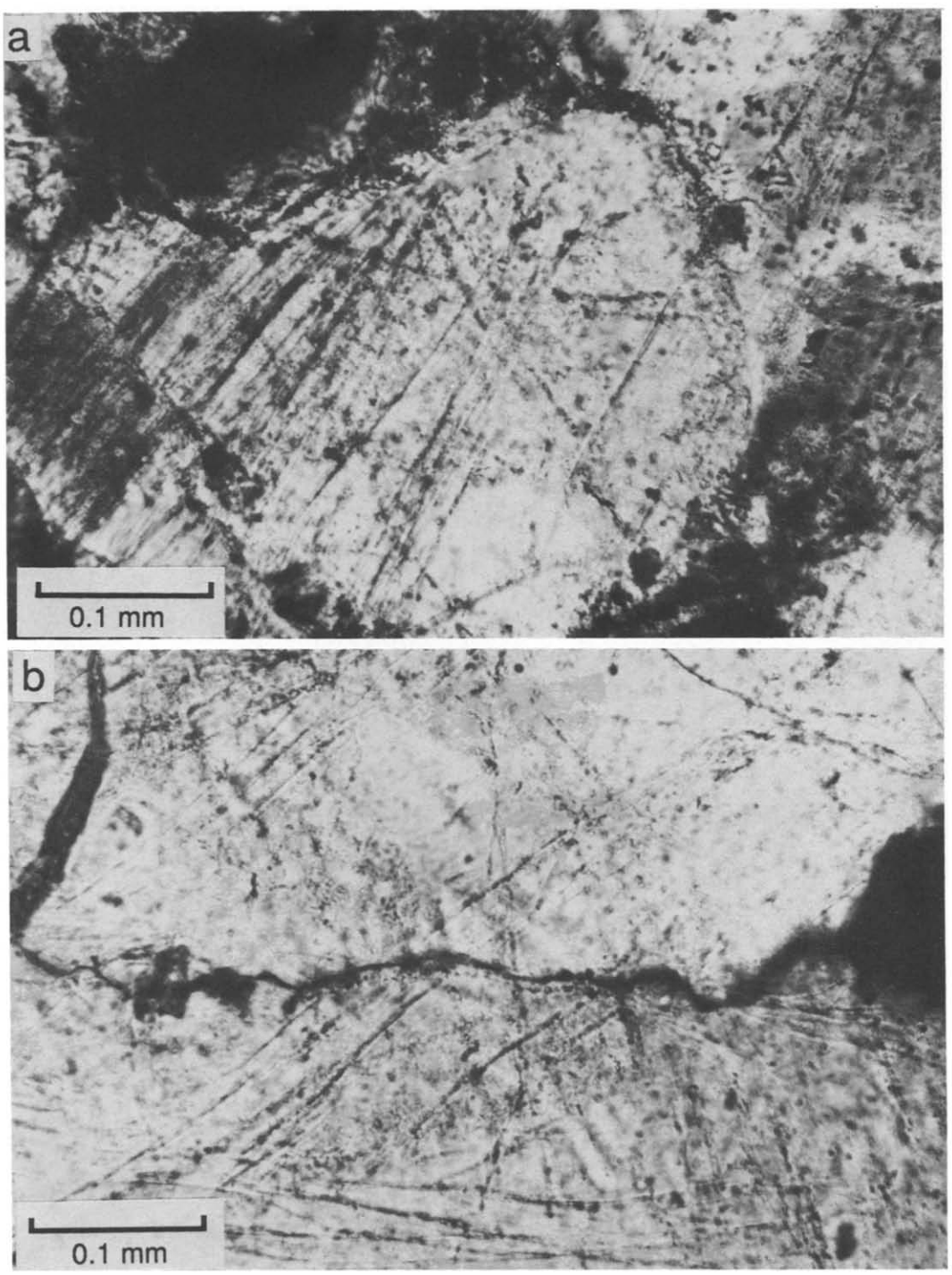

Fig. 6. (a) & (b) Photomicrographs of Lyons Sandstone. Photographs show a microfracture pattern that crosses grain boundaries.

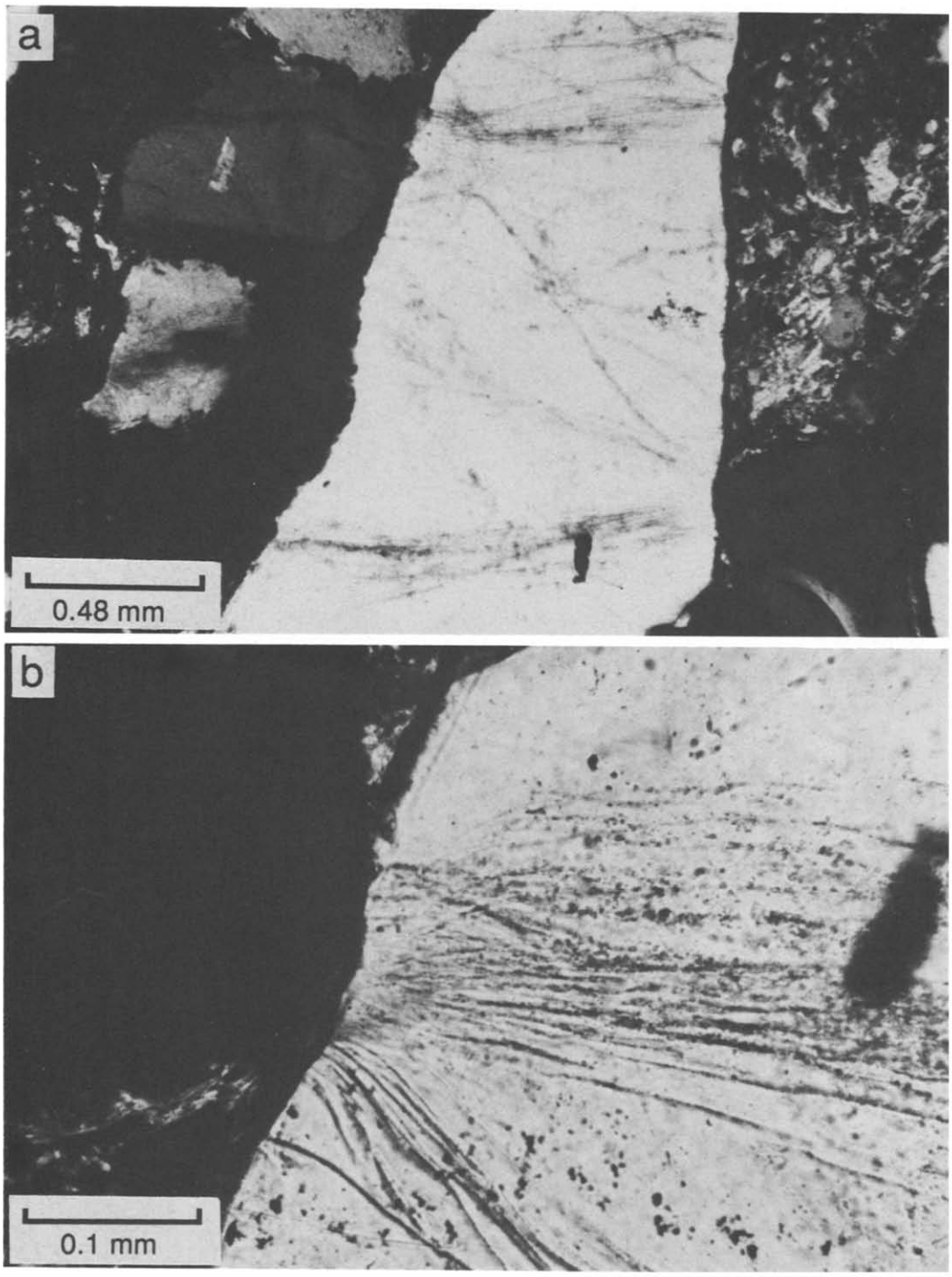

Fig. 7. (a) & (b) Photomicrographs of Fountain Formation arkose. Photographs show microfractures radiating from points of contact between quartz grains.

to the fracture plane; therefore, each observer will have a different criterion for identifying a microfracture inclined at some angle to the viewing direction. Friedman (1963, 1969), Engelder (1974) and Brock & Engelder (1977) used a scheme of ranking individual grains according to the number of microfractures observed in each grain. This scheme generates a 'microfracture index' that ranges from 100 to 500. Although it is important to standardize microfracture measurements, all techniques, including ours, incorporate an operator bias. Despite this difficulty, comparisons from one location to another by the same operator should provide internally consistent results. We found that for the more densely microfractured samples, the standard deviation on multiple measurements is around 20% while less densely microfractured samples, such as the Entrada and Navajo sandstones, one standard deviation is about 10%.

Figures 8(a)–(c) and Table 1 give the microfracture density vs distance normal to the fault surface. The normal faults at Drotar Ranch represent displacements of 1, 2 and 6 m; at Arches National Park, a displacement of 67 m; and at Flagstaff Mountain, a thrust fault is displaced 1.5 km. Because the greatest variability in microfracture density occurs in proximity to the fault, the spatial variation in microfracture density in the Fountain Formation is clearest when shown with a log scale (Fig. 8b). These data show that the density of microfractures found near the Flagstaff Mountain thrust fault are less than the densities observed for the normal faults at Drotar Ranch. However, a direct comparison cannot be made because the normal faults were sampled in closer proximity than was possible for the Boulder thrust fault. An analysis of covariance suggests that if the thrust fault measurements were made at the same distance from the fault as the normal faults, the density of microfracture would be the same. This is further supported by the good fit to an exponential regression ($r = 0.92$) of the combined microfracture data from the Fountain Formation at Drotar Ranch and Flagstaff Mountain (Fig. 8c). Therefore, for these faults, microfracture density is independent of both fault displacement and type of fault.

The Arches National Park fault has an intermediate displacement. However, microfracture density data from this fault cannot be compared to the data from the Fountain Formation because the two rock types are significantly different.

Similar to the density data, the width of the fracture zone appears to be independent of displacement. Again, the high correlation coefficient for the combined data of the Fountain Formation suggests a common zero intercept and therefore independence of fault zone width from displacement for sampling sites taken normal to the fault plane at the location of greatest displacement. A better way to define the width of the zone of microfracturing than regressing the density data is to define it as the distance between the fault surface and the point where the microfracture density goes to background. Although a direct comparison between the width of the zone of microfracturing for the two sampling sites of Fountain Formation could not be done, a comparison of the width of this zone can be made between data from the compositionally similar Aztec (Brock & Engelder 1977), Navajo and Entrada sandstones. The inset diagram in Fig. 8(c) from Brock & Engelder (1977) shows the microfracture density in the Aztec Sandstone near a thrust fault with at least 24 and perhaps as much as 88 km of displacement. Although a different measurement scheme is used (for further discussion see section on "Microfracture and macrofracture density") the distance at which the microfracture density in the Aztec Sandstone goes to background is between 3 and 20 m. Similarly, the density goes to background between 3 and 18 m for our samples taken from the Navajo and Entrada sandstones at Arches National Park.

At Arches National Park, the microfracture data from the Navajo and Entrada sandstones show significantly lower densities at all distances than any of the faults studied. The Navajo and Entrada sandstones are also the least well indurated of the rocks studied and have the highest porosity (25%). Perhaps intragranular slip rather than intergranular cracking took place in these rocks.

Because the microfractures are preserved in, and the stresses are transmitted by, both quartz and feldspar crystals, their proportion of the total mineralogy should effect the microfracture density. Figure 8(d) shows a comparison of microfracture density vs mineralogy. There is no consistent correlation between the density and the percentage of quartz plus feldspar suggesting the mineralogical content does not effect the distance vs density relationship for each of the respective units sampled. However, samples from the Carmel Formation, the units between the Navajo and Entrada sandstones, all have quartz plus feldspar contents of less than 25% and all exhibited microfracture populations so low that the minimum of 67 microfracture measurements per thin section could not be achieved. There is an apparent threshold of quartz plus feldspar content below which microfractures are not produced in significant numbers. Above the threshold, grain-to-grain contacts are increased and microfractures are produced in large numbers. Variation in the mineralogical content above the threshold, as can be seen in Fig. 8(d), have little effect on the number of microfractures produced. The exact threshold level was not detected but lies between 25 and 50% quartz plus feldspar.

Microfracture density vs fault slip

In order to test the lack of correlation between fault displacement and the intensity of microfracturing in conditions where the rock types are the same, we measured microfractures adjacent to a small displacement normal fault and two smaller displacement faults that splay off of it. The larger fault is displaced 6 m (labeled 'B' in Fig. 4), the two smaller faults are offset 2 and 1 m (faults 'A' and 'B'), respectively. The test for dependency of microfracturing on fault slip is that the

fault with greater displacement should both have a greater microfracture density as a function of distance from the fault surface and should also have a wider zone of microfracturing. The samples with the greatest microfracture density (Table 1) are CFD-1, CFD-2 and CFD-37, yet these samples are closer to the minor faults than to fault 'B'. Figure 8(e) is a plot of microfracture density vs distance from fault 'B' (solid squares). When the same microfracture density data are plotted against the distance to their respective closest faults ('A', 'B' and 'C')

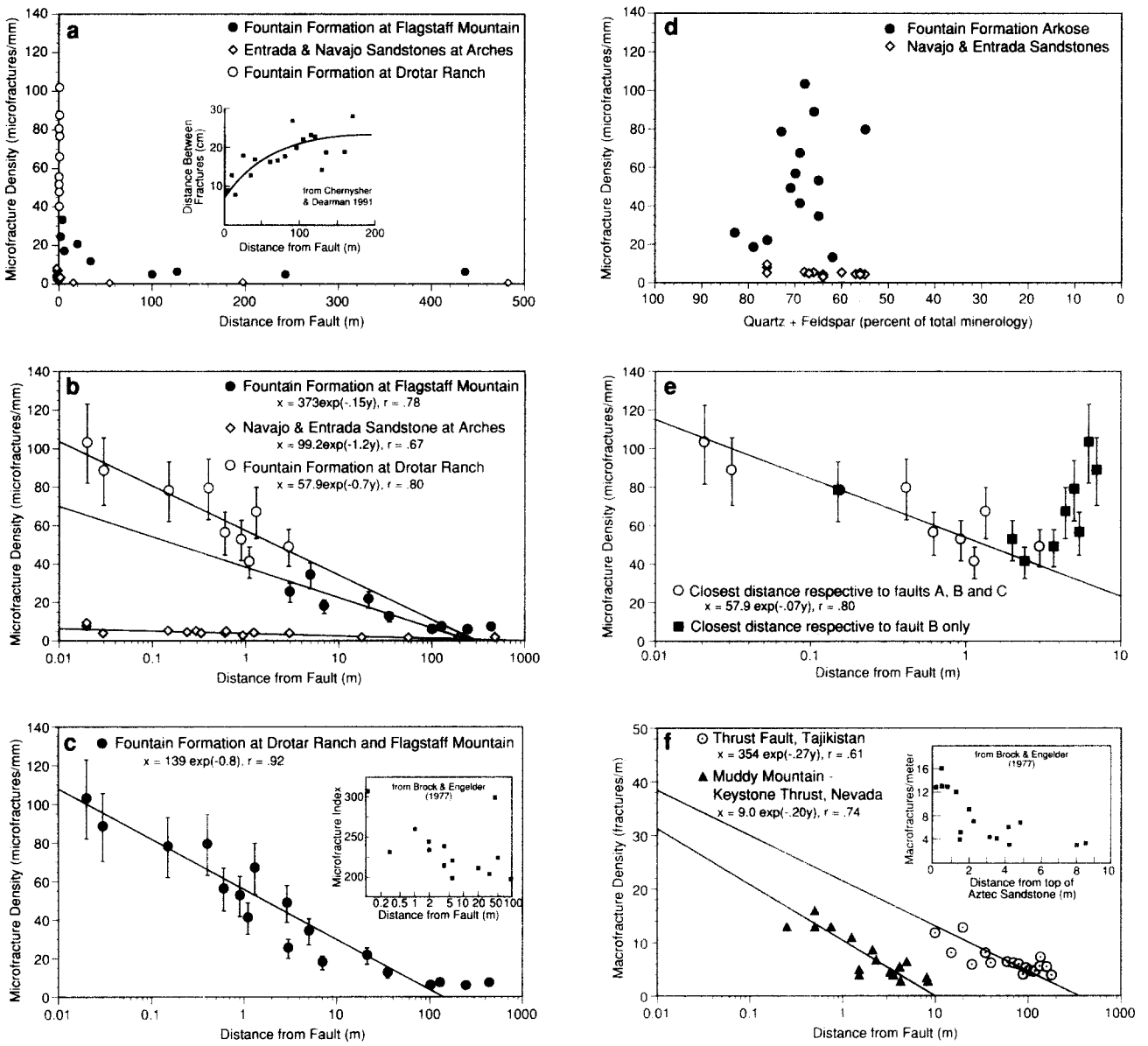

Fig. 8. (a) Microfracture density vs distance to the fault surface. Open circles are samples of the Fountain Formation arkose sampled in proximity to respective faults 'A' 'B' and 'C' at Drotar Ranch (see Fig. 4). Fault slip is 1, 6 and 2 m, respectively. Solid circles represent microfracture density measurements from the Fountain Formation at Flagstaff Mountain near the Boulder thrust fault west of Boulder, Colorado. Offset of the Boulder fault is determined to be 1.8 km. Open diamonds are the combined samples of the Navajo and Entrada sandstones taken near normal fault, with 67 m off-set, at Arches National Park. Inset is the macrofracture density vs distance from the fault surface for a thrust fault in central Russia with 0.8 km of displacement (from Chernyshev & Dearman 1991). (b) Microfracture density vs log-distance to the fault surface. (c) Microfracture density vs distance to the fault surface for the combined Fountain Formation arkose sampled at Drotar Ranch and Flagstaff Mountain. Inset diagram from Brock & Engelder (1977) show microfracture density of the Aztec Sandstone from the footwall of the 24 km Muddy Mountain–Keystone thrust fault of southern Nevada. Our microfracture data is not directly comparable to Brock & Engelder's because we measured microfractures directly where as Brock & Engelder used a microfracture index based on grouping individual grains into bins according to a range of microfractures counted for each grain. (d) Plot of microfracture density vs percent of quartz plus feldspar for the Fountain Formation arkose (solid circles) and Entrada and Navajo sandstones (open diamonds). (e) Microfracture density vs distance from fault surfaces at Drotar Ranch. Open circles are density vs distance from respective faults 'A', 'B' and 'C' shown on Fig. 4. The solid squares are the same microfracture density measurement but the distance to the fault surface is measured with respect to fault 'B' only. The farthest solid square to the right of this diagram is sample CFD-5 in Fig. 4 and is also the location of an open circle because fault 'B' is the closest fault to that sampling site. (f) Macrofracture density vs distance from the fault surface for fractures measured near a thrust fault with an off-set of 0.8 km located in central Russia (from Chernyshev & Dearman 1991) and fractures density in the Aztec Sandstone near the 24 km Muddy Mountain–Keystone thrust of southern Nevada.

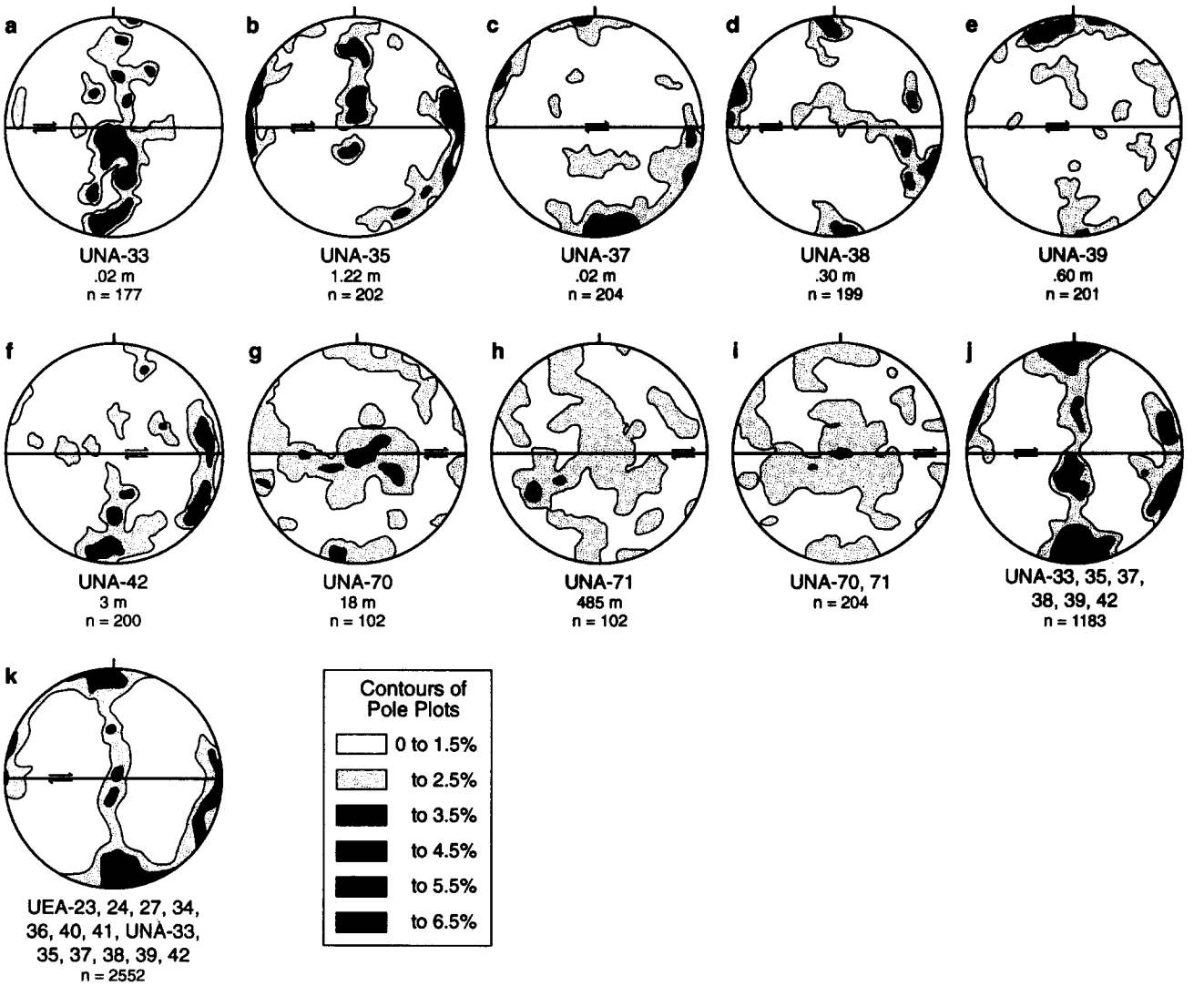

Fig. 9. (a)–(k) Contour plots of poles to microfractures for the Navajo Sandstone at Arches National Park. (i) Composite of diagrams (a)–(f). (k) Composite of diagrams (j) and Fig. 10(k). (i) Composite of (g) & (h). All diagrams are equal-area stereonets viewed parallel to the fault surface with the E–W direction corresponding to the slip direction. Arrows show sense of fault movement. The numbers below each diagram are the number of microfractures measured and the distance from the fault.

there is a clear relationship between distance and microfracture density. The distribution of solid squares in Fig. 8(e) suggest no relationship between microfracture density and distance to the fault surface. Although 'B' is the larger fault, it has no measurable influence on the microfracture density of the two smaller faults and therefore suggests an independence between net fault slip and microfracture density. Although the background microfracture density is not established at Drotar Ranch, independence between the width of the zone of microfracturing and displacement can be inferred by the fit of the regression of density as a function of distance to individual faults (open circles in Fig. 8e).

Microfracture orientation data

The most common orientation of microfractures is subparallel to the fault plane (Figs. 9, 10, 11 and 12). The exception are those samples that are judged to represent background microfracturing based on near random microfracture orientations (e.g. Figs. 9g, h & i, 10h, i & j, 11f, g, h & i and 14a & b) and uniform microfracture density (e.g. sample from greater than 100 m in Fig. 8c). Many of the individual sites sampled exhibit more than one concentration. For example, the stereonet for the sample nearest the fault in Arches National Park (sample UNA 37, Fig. 9c) exhibits one concentration parallel to plane of the fault and another concentration about 70° from the fault surface. Stepping out a few centimeters from the fault, the results for site UNA 33 (Fig. 9a) show a pronounced girdle of poles normal to the fault slip direction but not necessarily normal to the fault surface. The next site away from the fault (UNA 38, Fig. 9d) returns to that of the first sample. Therefore, there is significant variability from site to site which does not permit confident conclusions about the orientation of microfractures from a single site sampled close to this particular fault. For this reason, we have combined data sets for sites less than 3 m at the fault at Arches National Park and 35 m and less from the Boulder fault (Figs. 9j & k, 10k, 11j and 13e) and combined the data for samples taken at greater distances from these two localities (Figs. 9j, 10i and 14a & b). The combined data from the sites closer to the fault clearly show that the most prominent

orientation is at a low angle to the shear surface, irrespective of the particular fault or lithology. Composite Fig. 9(k) represents the largest number of microfracture orientations, all from samples within 3 m of the Arches National Park fault; the highest density of microfractures on this diagram is located 7° away from the shear plane; shear plane poles would be located on the top and bottom of the diagram. In composite Fig. 9(k) there is a skewing of microfractures away from the shear plane in the same sense as fault movement, or in a counterclockwise direction. Composite Figs 9(k), 10(k) and 13(e) also exhibit a skewing of microfractures that form a girdle between the centers of highest density. In almost every composite figure the peripheral skewing of poles is in the same sense of direction as fault movement. The only exceptions are samples CFD-5 and CFD-39.1 (Figs. 12g & d).

Effects of multiple faults

In order to test how the microfracture orientation is modified in a complex fault zone, we have again used the faults at Drotar Ranch (Figs. 3 and 4). Here, sampling was done such that we could tell if the microfracture orientation is specific to the individual faults or uniform throughout a region of faulting. One would predict that if multiple faults have overlapping fracturing zones, then the resultant microfracture pattern for a sample taken within the zone of overlap would have more than one distinct cluster group corresponding to respective faults. The overlapping faults include the Blue Mountain fault and Drotar Ranch faults 'A', 'B' and 'C'. The Blue Mountain fault is less than 100 m from the sampling site for the Drotar Ranch fault. Both faults may intersect at depth although the surface traces do not (Fig. 4). The microfractures sampled in the vicinity of the three smaller faults are shown in Figs. 12 and 13. There is not a definitive pattern of clustering associated with the Blue Mountain fault (see 'X' on stereonet diagrams in Figs. 12 and 13). Only in samples of the Lyons Sandstone (Fig. 13) is there even a suggestion of coincidence between the pole to the Blue Mountain fault and microfracture clusters.

Microfracture orientation populations of samples from the Fountain Formation at Drotar Ranch do not appear to overlap from one fault to another. In Figs. 12

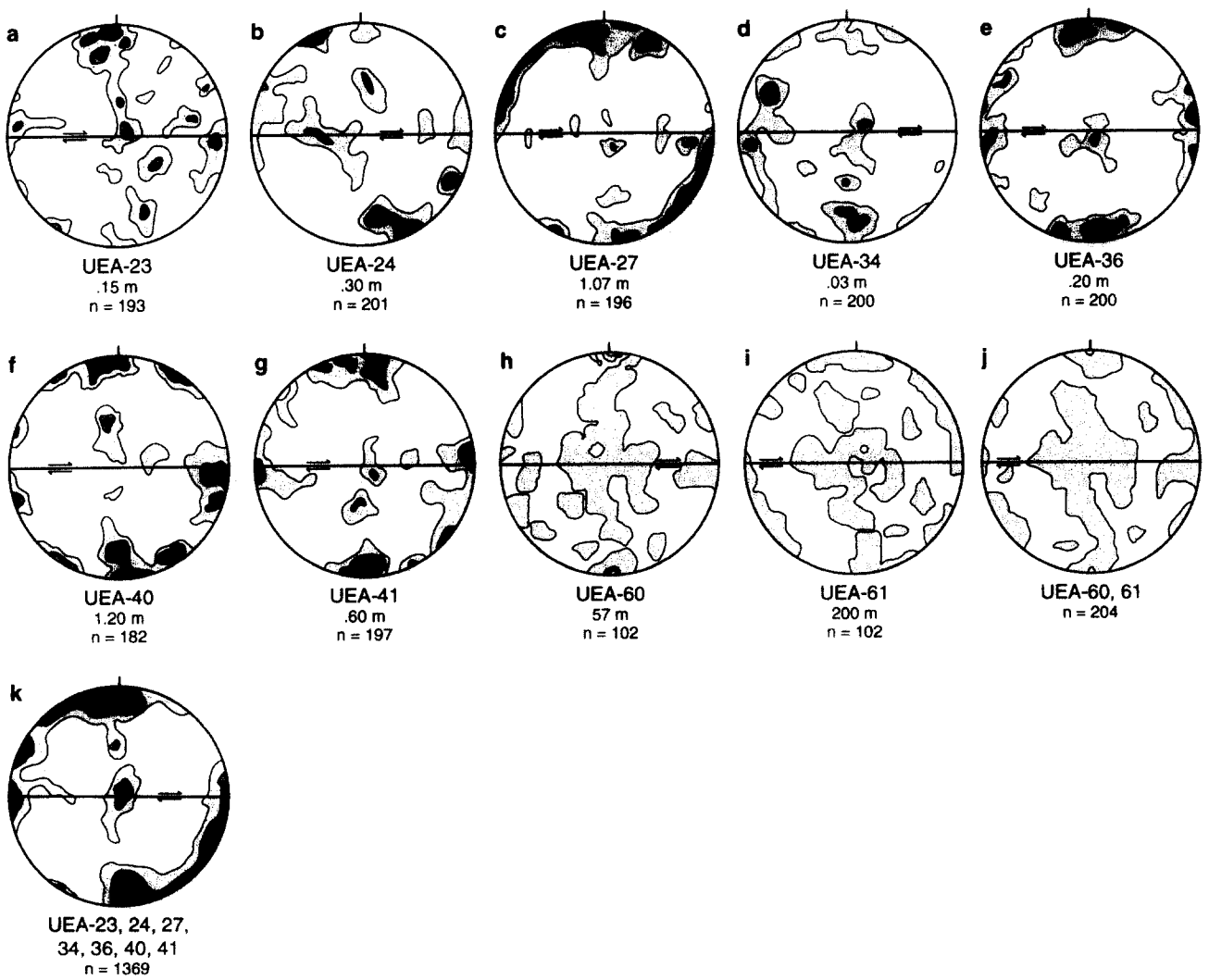

Fig. 10. (a)–(k) Contour plots of poles to microfractures for the Entrada Sandstone at Arches National Park. Contour intervals are the same as in Fig. 9. (k) Composite of diagrams (a)–(g). (j) is a composite of diagrams (h) and (i). See figure caption for Fig. 9 for further description.

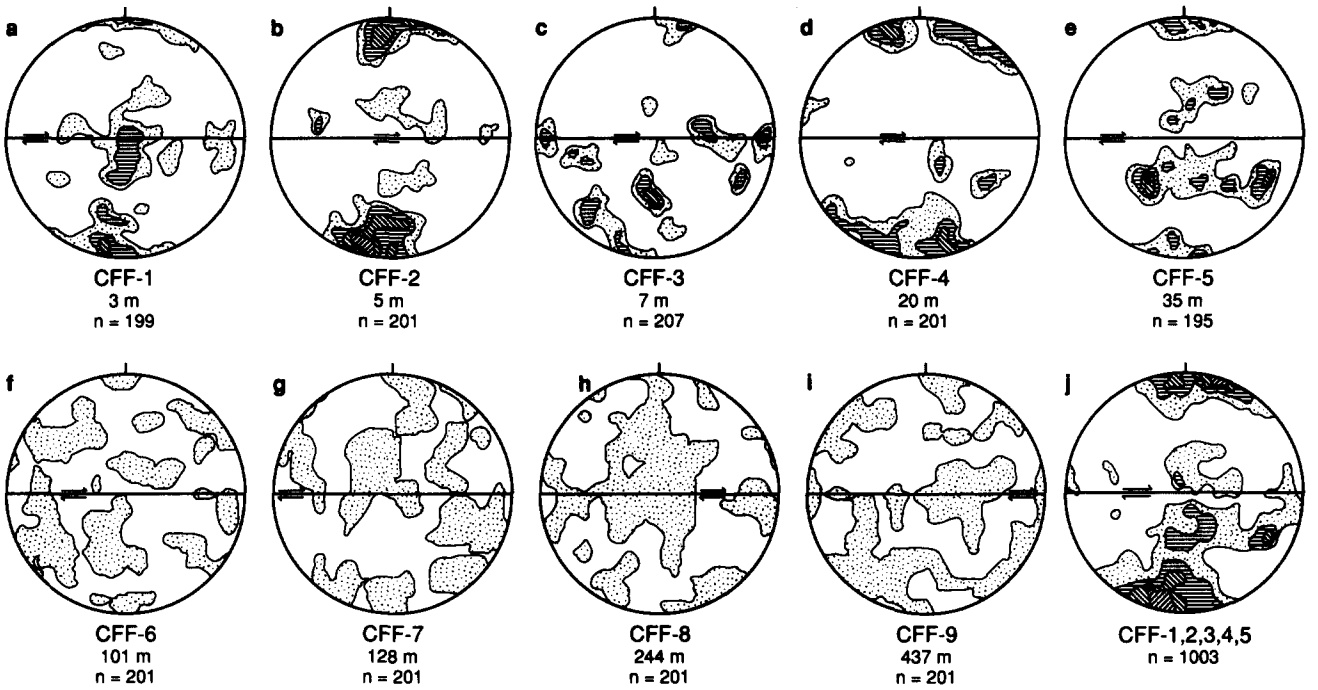

Fig. 11. (a)–(i) Contour plots of poles to microfractures of Fountain Formation arkose taken from near the Boulder fault on Flagstaff Mountain. Contour intervals are the same as in Fig. 9. (j) Composite of diagrams (a)–(e). Composite of (g), (h) & (i) is given in Fig. 14(b). See figure caption for Fig. 9 for further description.

and 13, poles to the respective fault surfaces do not correspond with or influence the location of microfracture clusters. Samples of the Fountain Formation in Figs. 12(f) & (g) are the only ones where there is a possible correlation between microfracture clusters and fault surfaces of other faults. The pole to the fault surface of the larger Blue Mountain fault, here displaced 30 m, only correlates with microfracture clusters in CFD-5 (Fig. 12).

The pole to the Blue Mountain fault does correlate with microfracture clusters in several samples of the Lyons Sandstone (Fig. 13). However, because a correlation is only observed for one rock type at Drotar Ranch, we will entertain the possibility that the position

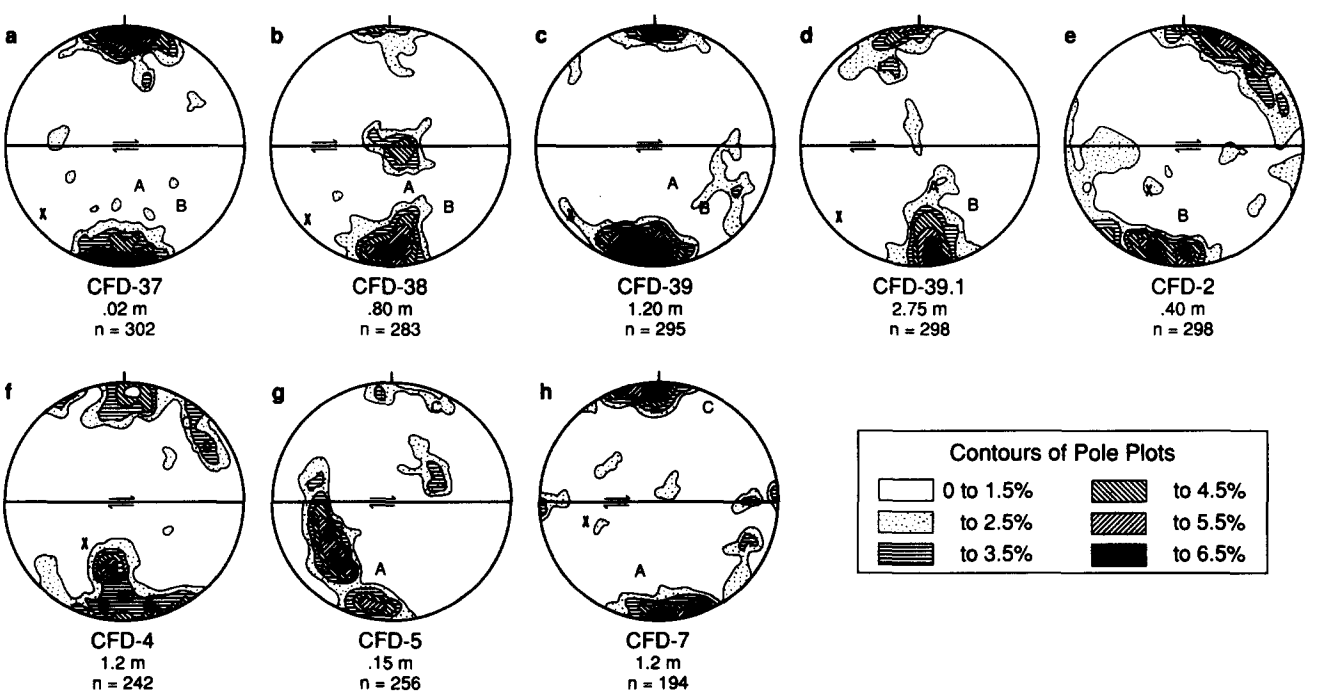

Fig. 12. (a)–(h) Contour plots of poles to microfractures for Fountain Formation arkose taken at Drotar Ranch. (a)–(d) were taken from near fault 'C'. (e) & (f) were taken from near fault 'A'. (g) & (h) were taken from near fault 'B'. Symbols for the poles to the shear surfaces of the other faults at Drotar Ranch are: an 'A' for fault 'A', a 'B' for fault 'B', a 'C' for fault 'C' and an 'X' for the pole to the Blue Mountain fault. See figure caption for Fig. 9 for further description.

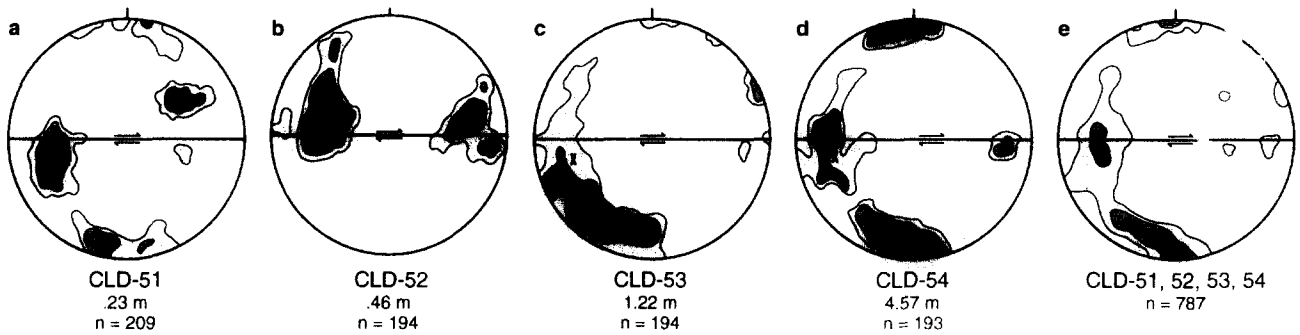

Fig. 13. (a)–(c) Contour plots of poles to microfractures from the Lyons Sandstone at Drotar Ranch. Contour intervals are the same as in Fig. 12. (e) is a composite of (a)–(d). All samples were taken from the hanging wall of fault 'B'. The 'X' corresponds to the location of the pole to the shear surface of the Blue Mountain fault. See figure caption for Fig. 9 for further description.

of the pole of the Blue Mountain fault in the Lyons Sandstone is coincidental and the orientations of microfractures in the Lyons Sandstone samples are controlled by something other than the extant stress field during formation of the Blue Mountain fault. The Lyons Sandstone samples were taken from the hanging wall of fault 'B'. Samples CFD-2 and CFD-5 were also sampled from the hanging wall of their respective faults. In Figs. 12 & 13 microfractures within samples taken from the footwall exhibit clusters that are fault-parallel. By contrast, microfractures within samples taken from the hanging wall correspond to microfractures oriented perpendicular to the fault surface.

DISCUSSION

Microfracture density

Although the kinematics of dilatancy and microfracturing in experimentally induced failure is well known (e.g. Bombolakis 1964, Brace *et al.* 1966, Scholz 1968, Hallbauer *et al.* 1973, Lockner & Byerlee 1977), there is still debate about the subsequent post-failure production of microfractures during fault slip. Brock & Engelder (1977) indicate that fault drag during the early stages of faulting is a major contributor to cataclasis, such as microfractures, near the faults they studied.

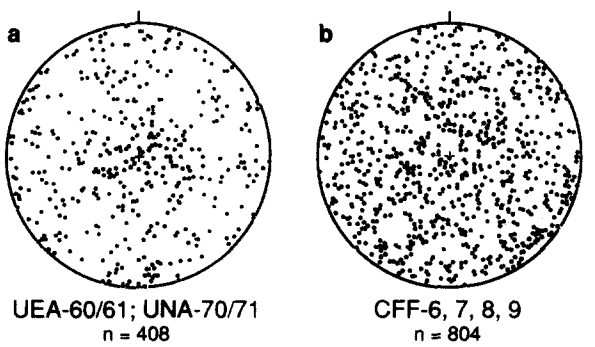

Fig. 14. Poles of microfractures from the four most distal sampling sites at (a) Arches National Park and (b) Flagstaff Mountain. Sampling distances from the fault surface range from 18 to 485 m for the Arch National Park normal fault and range from 101 to 437 m from the fault surface of the Boulder thrust fault at Flagstaff Mountain. For individual site data see Figs. 9, 10 and 11.

They describe a sequence whereby drag induces cataclasis that in turn acts to harden surrounding rock. As the surrounding rock becomes further indurated, slip is restricted to the fault contact. We distinguish microfractures from other forms of cataclasis such as the generation of gouge that has been shown from field observations (Wallace & Morris 1979, 1986, Robertson 1982) and in laboratory experiments (Teufel 1981, Yoshioka 1986) to increase with increasing displacement. Although variability in this relationship has been noted (e.g. Engelder 1974), Scholz (1987) has noted that the relationship between gouge thickness and slip exhibits a linear scaling. Additionally, we define the region of fracturing produced by the stress field at the time of earliest formation of a through-going fault as a process zone. We distinguish fractures formed in the process zone from those produced after significant displacement (typically greater than several meters) has accrued. The width of the process zone and the amount of displacement that defines the 'earliest formation' are dependent on the rock type and state of stress at failure.

Friedman & Logan (1970), Conrad & Friedman (1976) and Teufel (1981) further support this interpretation with experimental data showing that microfracture density increases as a function of fault displacement. In Teufel (1981) a plot of density vs displacement shows that as displacement increases, so does microfracture density. However, these data are for small (<1 cm) displacements which may be representative of the formation of a process zone. Although some microfracturing is no doubt produced as fault displacement increases, we suggest that the differential stress during initial failure seems to dominate the production of microfractures in the rocks we have studied. This idea is supported by observations of faulting in rocks having similar composition and porosity. For example, sampling of the Fountain Formation on the Drotar Ranch faults (Fig. 4) tested the dependence of microfracture density on displacement. As discussed in the results section, when samples from smaller faults (<2 m) are compared to faults with greater than 6 m displacement, there is no correlation between distance from the fault (fault 'B' in Fig. 4) and microfracture density (solid squares in Fig. 8e). This suggests to us that, even though each of these faults presumably experienced a similar

far-field stress at the time of failure, (1) the greater displaced fault continued to grow at the expense of the smaller faults, and (2) continued growth had little effect on the production of microfractures. It is important to note that these samples were all taken near the location of the maximum displacement and that we would expect that samples taken near the fault tips might not show a similar independence of fault length and process zone width. Moreover, smaller displaced faults at Drotar Ranch exhibit greater microfracture density than the 1.5 km displaced Flagstaff Mountain fault.

Differences in microfracture density between experimental and field data may in part be due to how microfractures are characterized. Friedman & Logan (1970) discuss what they call 'feather' microfractures as tensional microfractures. These microfractures form adjacent to fault surfaces as a result of initial displacement along the fault. They locally dominate any count of microfractures on the scale of an experimental sample. In our study, microfractures that open onto a shear surface occurred in only a few grains of the thousands we observed.

A possible reason for the observed greater microfracture density in samples from near the < 6 m displacement Drotar Ranch normal faults as compared to the lesser microfracture density near the 1.5 km displacement Boulder thrust is that we were not able to sample as close to the fault surface at Flagstaff Mountain as we were at Drotar Ranch. Contrasts in differential stress at failure and pore pressure may contribute as well. Since an exponential regression of the combined data sets yields $r = 0.92$, we suspect that the pattern of both density and width of the process zone for both faulting localities is the same. Although we did not observe significant granulation of rock beyond a few centimeters from the fault surface, reductions in grain size have been observed several meters away from the Muddy Mountain–Keystone thrust fault, which has an estimated displacement of 24 km (Brock & Engelder 1977). The observations of Brock & Engelder suggest that some deformation outside of the region where fault gouge is produced results from continued fault displacement.

Comparison of microfractures to macrofractures

Here, we would like to examine the relationship between the intensities of microfracturing and macrofracturing as a function of distance from the fault surface. Although the mechanisms of formation between the two are different for the same faulting episode, both are formed in response to the same stress fields in the same rock type under the same temperature and fluid pressures. The value in establishing such a relationship would lie in the ability to characterize the macrofracture network near a fault by measuring the microfracture density at a few locations, such as might be done in the limited recovery of drill cores. Because measurements of macrofracture density were not possible for the faults we studied, we have examined changes in the density of microfracturing and macrofracturing observed in proximity to two upper crust faults examined by other workers.

Brock & Engelder (1977) reported that macrofracture and microfracture density both decreased normal to the Muddy Mountain–Keystone thrust fault. The decrease in microfracture density is similar to that found in our study although the displacement of the Muddy Mountain–Keystone fault is 24 km. Our microfracture density values become statistically indistinguishable from background at from 3 to 18 m whereas theirs does so between 3 and 20 m. A somewhat different fall-off is observed for macrofracture data from the Muddy Mountain–Keystone fault as compared to microfracturing along the same traverse (Figs. 8c & f, insets). Macrofracture data from their study (Fig. 8f, inset) show a fall-off to background between 3 and 8 m. Although there is a narrower zone of macrofracturing compared to that for microfracturing in the Brock & Engelder (1977) study, in both their study and ours density of fracturing decays exponentially as a function of distance from the fault surface.

Macrofracture data from a thrust fault (displacement 0.8 km) near the Nurek Reservoir in Tajikistan (Chernyshev & Dearman 1991) show a similar exponential fall-off as the Muddy Mountain–Keystone thrust macrofracture data (Fig. 8f and inset in Fig. 8a). However, the width of the Tajikistan thrust fault is 300 m compared to a width of 10 m for the Muddy Mountain–Keystone thrust (Fig. 12), based on the zero intercept of the regression of fracture density. A reversed relationship between slip and fracture density is also observed in our data between the 67 m displaced Arches National Park normal fault and the maximum 6 m offset on the Drotar Ranch fault. However, the form of the macrofracture fall-off from these studies is the same as the form of the microfracture fall-off data from our study. The similarity in form of the fall-off between microfractures and macrofractures suggests that a scaling between the two can be established. So far the only data available for the same rock type and in the same faulting conditions are those of Brock & Engelder (1977). Differences in macrofracture density between the Tajikistan thrust and Muddy Mountain–Keystone thrust as well as differences in the two microfracture studies (Brock & Engelder's and ours) are likely due to the different rock types, pore fluid and stress conditions at the time of failure. Currently, a more thorough study of the relationship between microfracturing and macrofracturing is needed. But, the data presented here suggest, but do not verify, that the fracture network which may control fluid migration can be estimated by measuring the microfracture density in just a few locations.

Interpretation of microfracture orientation patterns

One of the more interesting observations of our study is the dominance of microfractures oriented subparallel to the fault plane. We also observed that a smaller subset of the microfracture population is oriented normal to the

fault surface. At Drotar Ranch, the only location where both sides of the fault were sampled, there is an asymmetry of microfracture orientation between footwalls and hanging walls. These observations were surprising to us because the microfractures in proximity to the faults we studied are tensional fractures and therefore parallel the orientation of the greatest principal stress σ_1. One would initially expect the far-field stress orientation to be about 30° from the fault surface assuming a Coulomb–Mohr fracture criterion. The near parallelism of the microfractures to the shear surface, as well as the subpopulation oriented normal to the fault plane, requires a local orientation of the stress field during the growth of a fault.

Our observation of the independence of microfracture density from fault slip leads us to conclude that the microfractures are early manifestations of faulting. The orientation data lead us to conclude that the microfractures were produced by a local stress field. These two observations together suggest to us that the preponderance of microfractures were formed near the leading edge of a propagating mode II or III fault tip.

Lawn & Wilshaw (1975) calculated stress orientation and magnitude within the region of a propagating tip of a mode II fracture and showed that σ_1 is oriented parallel to the shear surface within the region of compression and perpendicular to the shear surface within the region of tension. For a mode III fracture the σ_1 orientation would be parallel on both sides of the fault. In other words, the distribution of mode II fractures is asymmetrical with respect to the shear surface. For mode II, tension fractures are parallel to the plane of a propagating fault on the compressional side and normal to the fault plant on the tensional side. In mode III, both sides of the fracture are in compression and tensional fractures should lie parallel to it. Figures 15(a) & (b), taken from Scholz *et al.* (in press), show the calculated stress field around a propagating mode II fracture and the expected orientation of fractures produced within the stress field. Note that the microfracture orientations from our data closely resemble the fracture orientation in these figures.

Sampling of the Boulder thrust fault was done near its point of maximum displacement. Assuming that this fault propagated from depth upward relative to its present surface exposure, the Boulder thrust propagated as a mode II fracture past the sampling site. For a thrust fault, the upper plate will be in compression parallel to the fault surface. Only the upper plate of the Boulder thrust was sampled. Nevertheless, the orientation of microfractures there are subparallel to the thrust as would be consistent of a upward propagating mode II fracture.

The Arches National Park normal fault was sampled near its southeasternmost tip. This sampling site could be in a region that experienced a propagating mode III fracture, but this cannot be fully assessed until the full dimensions of the fault are known. However, the orientations of the microfractures are uniformly fault-subparallel orientation in both the hanging wall and

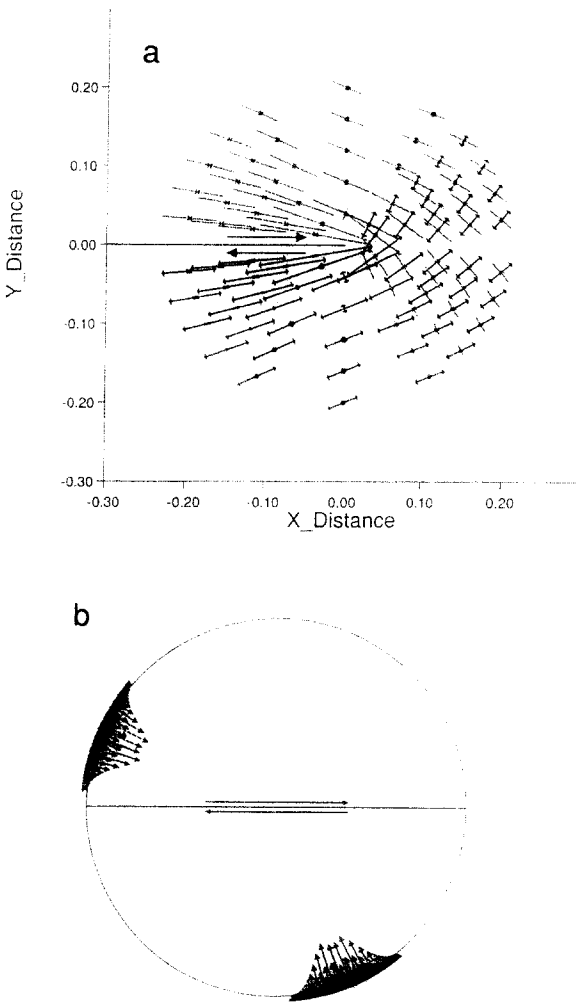

Fig. 15. (a) Plot of the principal stresses surrounding a mode II crack. Distances are normalized crack half-lengths. Compressions are shown in dashed lines with inward arrows, tension directions are solid lines with outward arrows. (b) Arrows on the stereonet indicate crack density as a function of crack orientation with respect to fault plane. Note that the microfracture orientations in our figures are poles to fractures and in this figure fractures are represented by the strike direction. Modified from Scholz *et al.* (in press).

footwall, as would be expected of microfractures formed in a location that has experienced passage of a mode III fracture.

Because of the small displacements on the Drotar Ranch faults, it cannot be determined whether or not sampling was done in the region of compression or tension or even whether the fault propagated in mode II or mode III. Although the direction of fault propagation cannot be precisely determined, it is worth noting that: (1) samples CFD-2, CFD-5, CLD-51, CLD-52, CLD-53 and CLD-54 (Figs. 12 and 13) all exhibit strong clustering of poles to microfractures normal to the fault plane or in the lower left quadrant of their respective stereonets; (2) all these samples are from their respective hanging walls; and (3) all other samples at Drotar Ranch are from their respective footwalls. This is the microfracture pattern expected for a mode II fracture propagating from depth up to the sampling locality. Because of the inability to define the direction of fault propagation at Drotar Ranch, we do not place much confidence in the meaning of microfracture clustering at this location.

However, the microfracture orientations from this location are consistent with, as are the microfracture data from the other sampling sites, a migrating fault tip stress field model.

If, as we suggest, the majority of fractures are formed in proximity to the fault tip, then the orientation of microfractures should be consistent with the stress field associated with the tip of propagating fault as predicted by Lawn & Wilshaw (1975). There are other possibilities that can account for the observed orientation of microfractures in our study, but our preferred interpretation is that microfracture orientation represents the stress field near a propagating mode II or mode III fault tip and not the far field stress orientation as is often assumed.

Skewing of microfracture cluster. Engelder (1974) observed skewing of microfracture poles away from centers of high microfracture density. He concluded the skewing is the result of grain rotation. Similar patterns of horizontal girdle skewing are evident in data from this study. For example, skewing is present on stereonets in Figs. 9(c), (f), (j) & (k); 10(c), (g) & (k); 12(e) & (h) and 13(c), (d) & (e). Assuming that grain rotation is the cause, the skewing in these figures is consistent with the sense of direction of fault movement (see arrow on fault surface). On composite diagram of the Entrada and Navajo sandstones (Fig. 9k) the skewing is represented by maxima in both the upper-left and lower-right quadrants of respective stereonets. In Fig. 10(k) the sense of expected rotation, as indicated by the movement arrow, is in a counter-clockwise direction. Skewing occurs most often within samples taken less than 3 m from the shear surface. Apparent rotated grains constitute only a few percent of the total population of grains and no sample taken from farther away than 3 m from the fault exhibited skewing. Most of the skewing occurs in samples from the Entrada and Navajo sandstones although some samples from other units exhibit similar patterns. Sample CFD-2 (Fig. 12e) is the only Fountain Formation sample to exhibit a horizontal skewing pattern similar to samples from the Entrada and Navajo sandstones. This sample also contains 43% hematite plus calcite, which is more typical of samples from the Entrada and Navajo sandstones than from the other units studied (Table 1). Samples CLD-53 and CLD-54 (Figs. 13c & d) of the Lyons Formation from Drotar Ranch show a similar skewing that could be due to grain rotations although the position of the pole for the Blue Mountain fault could just as well control the position of clustering. This is especially true for sample CLD-54 (Fig. 13d) where the cluster near the Blue Mountain fault's pole is isolated from the other clusters. Furthermore, these two samples contain 39 and 43%, respectively, of hematite plus calcite; again similar to the other samples that exhibit horizontal microfracture girdles. Except for those samples in which skewing correlates with the pole to the shear surface from neighboring faults, skewing is more prevalent in those samples that are higher in authigenic cement content and have fewer quartz overgrowths and are thus less well indurated. However, examination of individual thin sections show no indication of grain rotation. Only one thin section showed any sign of cataclasis other than the presence of microfractures. It is difficult to imagine a way in which only a few grains rotate within a much larger population yet leave no observable evidence of having done so.

Another possible explanation for the skewing is that it is not due to rotation of grains but rather due to changes in the local stress field as the propagating fracture tip passes through the area sampled. As the fault tip migrates past a sampling site during fault growth, σ_1 will change from being fault parallel or perpendicular, as predicted by the model of Lawn & Wilshaw (1975), to the far-field orientation of approximately 30°. If most of the microfractures are produced in the process zone, the dominant orientation will be fault parallel or perpendicular. After passage of the process zone, the newly formed microfractures will reflect the far-field stress orientation. The direction of skewing is consistent with this interpretation. From the above, we conclude that minor grain rotations could have occurred near the fault surface as was observed by Engelder (1974) and that mineral content is a significant factor although we cannot preclude rotations of the stress field as the fault grows.

Intermediate stresses. The skewing of microfracture poles in a girdle normal to the fault plane and parallel to the slip direction can be reasonably accounted for by either grain rotations or by the changing stress field near the tip of a propagating mode II or III fracture. However, the girdle of microfractures encircling the σ_1 direction, which appears in many of the stereonets (e.g. Figs. 9j & k and 10k), is not accounted for in either of these scenarios. We believe that the best explanation of the girdle of microfracture poles that encircle the σ_1 direction is a closeness in values of σ_2 and σ_3 during faulting. When σ_2 is significantly different from σ_3, poles of microfractures will be restricted to a girdle parallel to the slip direction and normal to the fault surface. If, on the other hand, σ_2 and σ_3 are the same, then the tensional cracks can have any orientation along a girdle normal to σ_1. But, when the values of σ_2 and σ_3 are close but not equal, a skewing of microfracture poles in a girdle normal to the σ_1 direction results, as exhibited in Figs. 9(j) & (k) and 10(k).

Zhao & Johnson (1992) have suggested, based on joint and fault sets, that the regional intermediate principal stress axis in Arches National Park was vertical. Because the depth of faulting was shallow (1.7 km, Cater 1970) the vertical and horizontal stresses could have been close in magnitude during faulting. This suggestion is best represented by the girdle of microfracture poles seen in combined data sets Figs. 9(j) & (k) and 10(k). This pattern is exhibited in most of the individual site stereonets for the Arches National Park fault as well as several from the Boulder fault, but not those for the Drotar Ranch fault. Therefore, it appears to us that the magnitudes of σ_2 and σ_3 were close in value at initial failure for the Arches National Park and Boulder faults,

and that stress values of σ_2 and σ_3 were significantly different at failure for the Drotar Ranch fault.

Background microfracturing. Samples for microfracture density and orientation were taken as far as 500 m from individual faults. As with the microfracture density data, the orientation data show marked changes as a function of distance from the fault. This is best seen when comparing composite diagrams from sites located within 3 m of a fault to sites located at greater distances. The composite diagram (Fig. 9k) for both the Entrada and Navajo sandstones within 3 m of the fault show a preferred orientation. However, microfracture measurements exhibit a random distribution for the same rock types sampled at distances between 18 and 485 m from the Arches National Park fault (Figs. 9g, h & i, 10h, i & j and 14a). In a similar comparison, samples of the Fountain Formation less than 35 m from the fault surface, show a strong preferred orientation of microfractures while samples from 101 to 437 m (Fig. 14b) approach a random distribution.

At both the Arches National Park fault and the Boulder fault, the distance from the fault at which a preferred orientation disappears is about the distance where the microfracture density falls off to a constant or background level. This implies that there is a large random component to the microfracture population at these two locations. Furthermore, the random component may mask any preferred orientation that is more weakly represented such as lithostatic loading or far-field stresses. Laubach (1988, 1989) detected such regional stresses in the East Texas basin with significantly fewer microfracture measurements than we have made. However, the Arches National Park sampling site has been subjected to several different regional stress fields through time, producing prominent sets of joints and strike-slip faults of various orientations as described by Zhao & Johnson (1992). These vertical joint sets and faults may be present as represented by a slight concentration of vertical microfractures (e.g. UNA-70, Fig. 9g). We have assumed these concentrations to be parallel to a vertical intermediate stress but they could just as easily be due to horizontal far-field maximum principal stress or they could just be statistical aberrations. To further complicate matters, the changing position of the stress field over time observed by Zhao & Johnson (1992) for this area may have contributed to the overall near random appearance of distal microfracture orientations at Arches National Park (Fig. 14a). Nevertheless, it is clear that samples taken near the fault plane dominate any random component in the microfracture orientation data we have presented.

Inherited microfractures. The large random component observed in the arkose and sandstone samples from Arches National Park and Flagstaff Mountain suggest that many of the microfractures were inherited from older deformed units. Of these two locations, there is a significantly higher contribution of background microfractures at Flagstaff Mountain (Table 1). Although the inherited contribution of microfractures is significant at sites such as Flagstaff Mountain, we believe that inherited microfractures have no inherent anisotropy and thus do not bias the conclusions drawn from our microfracture orientation or density observations. We base this interpretation on the following lines of reasoning. (1) Microfracture orientations are random away from the fault plane (Figs. 14a & b) and have strong preferred orientations near the fault plane. It is difficult to imagine how a grain deposited with preexisting microfractures could preferentially orient itself with respect to a fault that does not yet exist. (2) The density of microfractures is greater near the fault than away from it (Figs. 8a–e). A region of grains with preexisting microfractures could offer a zone of weakness through which a fault could propagate. However, the faults we studied cut across sedimentary horizons. (3) Samples of Lyons Sandstone exhibited a interlocking pattern of quartz grains and quartz overgrowths. The bulk of microfracture observed traverse grains and overgrowth, with numerous microfractures traversing several grains and associated overgrowths (see photomicrographs in Figs. 6a & b). All these suggest inherited microfracture do not significantly affect our results. The only important effect of inherited microfractures is in creating a low signal to noise ratio that subsequently requires large numbers of microfracture measurements in order to assess any preferred microfracture orientation or density pattern.

Microfracture and shear plane orientations

A noteworthy finding of this study is the small angle between the mean microfracture population and fault plane orientations. Most often the angle between the plane of the fault and mean plane of microfractures ranged from 5° to 20°. We prefer the interpretation that microfractures are produced in a process zone associated with a mode II or mode III propagating fracture. However, the following alternate explanations are plausible. (1) Microfractures may represent the orientation of the far-field σ_1 as has been interpreted experimentally (Hallbauer *et al.* 1973, Tapponnier & Brace 1976, Holcomb & Stevens 1980). Therefore, the low angle between σ_1 and the shear surface may mean that the shear strength of the rocks we studied were larger than what laboratory experiments indicate. (2) Assuming both a curvilinear failure envelope and low confining pressures for these upper crustal rocks, failure could have occurred at an orientation nearly parallel to the σ_1 axis. (3) A large 2θ related to high fluid pressures at the time of failure, resulting in an effective σ_3 in tension combined with a low value for σ_1. (4) Most of the microfractures are not the product of the initial propagating rupture but rather are later products of a maturing fault zone in which the stress field rotated near the established

shear surface during subsequent rupture events (see Friedman *et al.* 1976).

Evidence supporting high values of shear strength for rock at failure is sparse. Some suggestion comes from field studies of conjugate fault sets. Duschatko (1953) and Spencer (1959) reported large numbers of shear sets with dihedral angles ranging from 10° to 40°. Experimental evidence for high values of shear strength come from experiments that involve intermediate principal stresses. Mogi (1967) found that as the value of σ_2 increased, the angle between the shear surface and the maximum principal stress axis decreased. The lowest angle between the shear plane and σ_1 which Mogi found was 19° for a compression test on Westerly Granite. Aydin & Reches (1982, p. 111, fig. 6a) show that the angle between the shear plane and σ_1 is about 13° for samples of granite they deformed under polyaxial compression; other rock types they studied exhibited angles up to 25°. Both the experimental results of Aydin & Reches (1982) and our observations indicate the possible presence of both high values of shear strength and unique values of intermediate stress.

In order for high fluid pressures to explain the low angle between the shear surface and σ_1, the fluid pressures for all the sites studied must have been coincidentally high. There is little field evidence for high fluid pressures at these sites, but this does not rule them out.

There is also little experimental evidence to support a rotation of the principal stress axes near a pre-existing shear surface after passage of the initial rupture. However, Sadovsky & Nersesou (1974), using focal mechanism data, reported finding a rotation of principal stress axis just prior to large earthquakes. Engdahl & Kissinger (1977) reported similar findings for an Adak Island earthquake. Although an analogy between plate-boundary earthquakes and upper crustal faulting is conjecture, it is apparent that for both the above observations, some as yet unexplained phenomenon is required to produce such anomalous stress orientations. Moreover, a direct comparison requires the stress field orientation to reorient itself along a fully developed fault. The independence of microfracture density from fault slip suggest that the microfracture production is an early feature of fault development.

Another possibility for the small angle between shear surfaces and their associated microfracture orientations is that pre-existing joint sets controlled the orientation of the developing fault. Zhao & Johnson (1992) noted that joints within the Arches National Park area commonly served as future fault surfaces. The microfractures near the Arches National Park fault could have formed in response to the stress field that created a joint yet the stresses resulting in the transformation of the joint to a normal fault did not contribute significantly to the microfracture population. We do not prefer this scenario because the orientation of the fault is not consistent with the fracture sets observed by Zhao & Johnson. Moreover, there are no joint sets at the two other locations studied, yet there is a similar close correlation between microfractures and the fault surface.

Dugdale–Barenblatt model of fault propagation

The Dugdale–Barenblatt model (Dugdale 1960, Barenblatt 1962) is an elastic–plastic fracture mechanics model of crack-tip propagation. In their model, material beyond the crack-tip will deform elastically and material within the region of the tip will deform inelastically. The yield strength of the material and cumulative displacement controls the width of the process zone or zone of inelastic behavior. Moreover, the taper or length of the region of inelastic behavior increases as the fracture grows. For finite values of yield strength, the zone over which stresses are elevated will increase outward in proportion to the stresses acting on the tip of the fault. As the fracture grows, the region over which the yield strength is exceeded will grow linearly and the stresses will decay exponentially away from the crack tip.

Cowie & Scholz (1992) have suggested that the Dugdale–Barenblatt model of crack-tip propagation is applicable to the growth of naturally occurring faults. They suggest that the region of inelastic yield is analogous to the zone of fracturing surrounding a fault. Moreover, Scholz *et al.* (in press) argue that since the zone of inelastic yield increases with fault length, then longer faults should have wider fracture zones and that longer faults will be accompanied by a 'dog bone'-shaped distribution of fractures symmetric about the fault. They further argue by analogy that the density of fracturing should decay exponentially away from the fault surface.

The fall-off of microfracture density near the faults we studied exhibits an exponential decay in microfracture density as a function of distance from the fault surface (Fig. 8b). A regression performed on these data yield correlation coefficients of $r = 0.67, 0.78$ and 0.80 suggesting agreement with the Dugdale–Barenblatt model as applied to faults (Cowie & Scholz 1992). Furthermore, microfracture density and distribution is independent of displacement. Moreover, we interpret microfractures to have been produced in the early stages of fault growth in a process zone equivalent to the region of inelastic yield described in these models of crack and fault growth. However, our sampling of faults was restricted to those areas of the fault where the displacement was assumed to be the greatest and thus we cannot assess the prediction of a 'dog bone' fracture distribution. Nonetheless, the data presented here are consistent with the Cowie & Scholz (1992) model of fault growth.

CONCLUSIONS

Microfracture orientation and density distribution from three upper crustal faults indicate that microfracture density and fracture zone widths are independent of fault displacement. Furthermore, microfracture orientation data show that the angle between the microfractures and the fault plane was most commonly between 5° and 20°. One fault sampled exhibited microfracture orientations subparallel to the fault plane in the footwall

and a perpendicular orientation in the hanging wall. Although other explanations are possible, we interpret these microfracture orientation and density patterns to be the result of inelastic yield near the fault tip of a propagating mode II or mode III fracture. In the incipient process zone, the local orientation of the maximum principal stresses do not align with the far-field stresses but rather are predicted to align either symmetrically (subparallel on both sides of the fault) for mode III or asymmetrically (subparallel on one side and perpendicular on the other) for mode II.

Acknowledgements—We would like to thank B. R. Clark for his initial contributions to this study and we would also like to thank Roger and Pat Drotar for their generosity in allowing us access to their ranch. We would also like to thank Atilla Aydin, Dave Pollard, Mel Friedman, Marco Antonellini, Chris Scholz, Nancye Dawers and an anonymous reviewer for helpful comments and reviews. We would also especially thank Maureen Anders for help with the graphics. This work was supported by the NSF grant EAR90-04534 and ACS grant 24563 to MHA.

REFERENCES

Aydin, A. 1978. Small faults formed as deformation bands on sandstone. *Pure & Appl. Geophys.* **116**, 913–942.

Aydin, A. & Johnson, A. M. 1978. Development of faults as zones of deformation bands and as slip surfaces in sandstone. *Pure & Appl. Geophys.* **116**, 922–929.

Aydin, A. & Reches, Z. 1982. Number and orientation of fault sets in the field and in experiments. *Geology* **10**, 107–112.

Baker, A. A. 1933. Geology and oil possibilities of the Moab district, Grand and San Juan Counties, Utah. *Bull. U.S. geol. Surv.* **841**, 95.

Barenblatt, G. I. 1962. The mathematical theory of equilibrium cracks in brittle fracture. *Adv. Appl. Mech.* **7**, 55–80.

Bombolakis, E. G. 1964. Photoelastic investigation of brittle crack growth within a field of uniaxial compression. *Tectonophysics* **1**, 343–351.

Borg, I. Y,. Friedman, M., Handin, J. & Higgs, D. V. 1960. Experimental deformation of St. Peter Sand: A study of cataclastic flow. *Mem. geol. Soc. Am.* **79**, 133–191.

Borg, I. Y. & Maxwell, J. C. 1956. Interpretation of fabrics of experimentally deformed sands. *Am. J. Sci.* **254**, 71–81.

Brace, W. F. 1971. Micromechanics in rock systems. In: *Structure, Solid Mechanics and Engineering Design* (edited by Te'eni, M.). John Wiley and Sons, London, 187–204.

Brace, W. F. & Bombolakis, E. G. 1963. A note on brittle crack growth in compression. *J. geophys. Res.* **68**, 3709–3713.

Brace, W. F., Paulding, B. W. & Scholz, C. H. 1966. Dilatancy in the fracture of crystalline rocks. *J. geophys. Res.* **71**, 3939–3953.

Brock, W. G. & Engelder, T. 1977. Deformation associated with the movement of the Muddy Mountain overthrust in the Buffington window, southeastern Nevada. *Bull. geol. Soc. Am.* **88**, 1667–1677.

Cater, F. W. 1970. Geology of the Salt Anticline Region in Southwestern Colorado. *Prof. Pap. U.S. geol. Surv.* **637**.

Chernyshev, S. N. & Dearman, W. R. 1991. *Rock Fractures*. Butterworth-Heinemann, London.

Conrad, R. E. & Friedman, M. 1976. Microscopic feather fractures in the faulting process. *Tectonophysics* **33**, 187–198.

Cowie, P. A. & Scholz, C. H. 1992. Physical explanation for displacement-length relationship of faults using a post-yield fracture mechanics model. *J. Struct. Geol.* **14**, 1133–1148.

Dugdale, D. S. 1960. Yielding of steel sheets containing slits. *J. Mech. Phys. Solids* **8**, 100–115.

Dula, W. F. 1981. Correlation between deformation lamellae, microfractures, macrofractures, and *in situ* stress measurements, White River Uplift, Colorado. *Bull. geol. Soc. Am.* **92**, 37–46.

Dunn, D. E., LaFountain, L. J. & Jackson, R. E. 1973. Porosity dependence and mechanism of brittle fracture in sandstone. *J. geophys. Res.* **78**, 2403–2417.

Duschatko, R. W. 1953. Fracture studies in the Lucero Uplift, New Mexico. *U.S. Atomic Energy Comm.* **RME-3072**.

Engdahl, E. R. & Kisslinger, C. 1977. Seismological precursors to a magnitude 5 earthquake in the Aleutian islands (supplement). *J. Phys. Earth* **25**, 243–250.

Engelder, T. 1974. Cataclasis and the generation of fault gouge. *Bull. geol. Soc. Am.* **85**, 1515–1522.

Friedman, M. 1963. Petrofabric analysis of experimentally deformed calcite-cemented sandstones. *J. Geol.* **71**, 12–37.

Friedman, M. 1969. Structural analysis of fractures in cores from the Saticoy field, Ventura Co., California. *Bull Am. Ass. Petrol. Geol.* **53**, 367–389.

Friedman, M. 1975. Fracture in rock. *Rev. Geophys.* **13**, 352–358.

Friedman, M., Handin, J., Logan, J. M., Min, K. D. & Stearns, D. W. 1976. Experimental folding of rocks under confining pressure: Part III—faulted drape-folds in multilithologic layered specimens. *Bull. geol. Soc. Am.* **87**, 1049–1066.

Friedman, M. & Logan, J. M. 1970. Microscopic feather fractures. *Bull. geol. Soc. Am.* **81**, 3417–3420.

Gallagher, J. J. 1987. Fractography of sand grains broken by uniaxial compression. In: *Clastic Particles: Scanning Electron Microscopy and Shape Analysis of Sedimentary and Volcanic Clasts* (edited by Marshall, J. R.). 189–208.

Gallagher, L. L., Friedman, M., Handin, J. & Sowers, G. 1974. Experimental studies relating to microfracture in sandstone. *Tectonophysics* **21**, 203–247.

Hallbauer, D. K., Wagner, H. & Cook, N. G. 1973. Some observations concerning the microscopic and mechanical behavior of quartzite specimens in stiff, triaxial compression tests. *Int. J. Rock Mech. & Min. Sci.* **10**, 713–726.

Hancock, P. L. 1985. Brittle microtectonics: principles and practice. *J. Struct. Geol.* **7**, 437–457.

Holcomb, D. J. & Stevens, J. L. 1980. The reversible Griffith crack: a viable model for dilatancy. *J. geophys. Res.* **85**, 7101–7107.

Hoshino, K. 1972. Brittle fracturing of non-foliated rocks. Paper presented at 24th International Geologic Congress, Montreal.

Hubert, J. F. 1960. Petrology of the Fountain and Lyons Formation (sic), Front Range, Colorado. *Colorado School Min. Quart.* **55**.

Joesting, H. R. & Plouff, D. 1966. Regional geophysical investigations of the Moab–Needles area, Utah. *Prof. Pap. U.S. geol. Surv.* **516-C**.

Kanaori, Y., Yairi, K. & Ishida, T. 1991. Grain boundary microcracking of granitic rocks form the northeastern region of the Atotsugawa fault, central Japan: SEM backscattered electron images. *Eng. Geol.* **30**, 221–235.

Knipe, R. J. & White, S. H. 1979. Deformation in low grade shear zones in the Old Red Sandstone, S.W. Wales. *J. Struct. Geol.* **1**, 53–66.

Kowallis, B. J., Wang, H. F. & Jang, B.-A. 1987. Healed microcrack orientations in granite from Illinois borehole UPH-3 and their relationship to the rock's stress history. *Tectonophysics* **135**, 297–306.

Kranz, R. L. 1983. Microcracks in rocks: a review. *Tectonophysics* **100**, 449–480.

Laubach, S. E. 1988. Subsurface fractures and their relationship to stress history in East Texas basin sandstone. *Tectonophysics* **156**, 37–49.

Laubach, S. E. 1989. Paleostress directions from the preferred orientation of closed microfractures (fluid-inclusion planes) in sandstones, East Texas basin, U.S.A. *J. Struct. Geol.* **11**, 603–611.

Lawn, B. R. & Wilshaw, T. R. 1976. *Fracture of Brittle Solids*. Cambridge University Press, Cambridge.

Lespinasse, M. & Pecher, A. 1986. Microfracturing and regional stress field: a study of the preferred orientations of fluid-inclusion planes in a granite from the Massif Central, France. *J. Struct. Geol.* **8**, 169–180.

Lloyd, G. E. & Knipe, R. J. 1992. Deformation mechanisms accommodating faulting of quartzite under upper crustal conditions. *J. Struct. Geol.* **14**, 127–143.

Lockner, D. & Byerlee, J. D. 1977. Hydrofracture in Weber Sandstone at high confining pressures and differential stress. *J. geophys Res.* **82**, 2018–2026.

Lockner, D. A., Byerlee, J. D., Kuksenko, V., Ponomarev, A. & Sidorin, A. 1991. Quasi-static fault growth and shear fracture energy in granite. *Nature* **350**, 39–42.

Lohman, S. W. 1975. The Geologic Study of Arches National Park. *Bull. U.S. geol. Surv.* **1393**, 113.

Matthews, V., III & Work, D. F. 1978. Laramide folding associated with basement block faulting along the northeastern flank of the Front Range, Colorado. *Mem. geol. Soc. Am.* **151**, 101–124.

Mogi, K. 1967. Effect of intermediate principal stress on rock failure. *J. geophys. Res.* **72**, 5517–5531.

Robertson, E. C. 1982. Continuous formation of gouge and breccia during fault displacement. In: *Issues in Rock Mechanics* (edited by

Goodman, R. E. & Hulse, C.). American Institute of Mining Engineering, New York, 397–404.
Rowland, R. A. 1946. Grain-shape fabrics of elastic quartz. *Bull. geol. Soc. Am.* **57**, 547–563.
Sadovsky, M. A. & Nersesou, I. L. 1974. Forecasts of earthquakes on the basis of complex geophysical features. *Tectonophysics* **23**, 247–255.
Sangha, C. M., Talbot, C. J. & Dhir, R. K. 1974. Microfracturing of a sandstone in uniaxial compression. *Int. J. Rock Mech. & Min. Sci. Geomech. Abs.* **11**, 107–113.
Scholz, C. H. 1968. Microfracturing and inelastic deformation of rock in compression. *J. geophys. Res.* **73**, 1414–1432.
Scholz, C. H. 1987. Wear and gouge formation in brittle faulting. *Geology* **15**, 493–495.
Scholz, C. H., Dawers, N. H., Yu, J.-J., Anders, M. H. & Cowie, P. A. In press. Fault growth and fault scaling laws: preliminary results. *J. geophys. Res.*
Simmons, G., Todd, T. & Baldridge, W. S. 1975. Toward a quantitative relationship between elastic properties and cracks on low porosity rocks. *Am. J. Sci.* **275**, 318–345.
Spencer, E. W. 1959. Geologic evolution of the Beartooth Mountains, Montana and Wyoming, Part 2. Fracture patterns. *Bull. geol. Soc. Am.* **70**, 467–508.
Tapponnier, P. & Brace, W. F. 1976. Development of stress-induced microcracks in Westerly granite. *Int. J. Rock Mech. & Min. Sci. Geomech. Abs.* **13**, 103–112.
Teufel, L. W. 1981. Pore volume changes during frictional sliding of simulated faults. In: *Mechanical Behavior of Crustal Rocks, The Handin Volume. Am. Geophys. Un. Geophys. Monogr.* **24**, 135–145.
Tuttle, O. F. 1949. Structural petrology of planes of liquid inclusions. *J. Geol.* **57**, 331–356.
Wallace, R. E. & Morris, H. T. 1979. Characteristics of faults and shear zones as seen in mines in depths as much as 2.5 km below the surface. In: *Proc. VIII Conf. on Analysis of Actual Fault Zones in Bedrock. U.S. geol. Surv. Open-file Rep.* **79-1239**, 79–100.
Wallace, R. E. & Morris, H. T. 1986. Characteristics of faults and shear zones in deep mines. *Pure & Appl. Geophys.* **124**, 107–126.
Yoshioka, N. 1986. Fracture energy and the variation of gouge and surface roughness during frictional sliding of rocks. *J. Phys. Earth* **34**, 335–355.
Zhao, G. & Johnson, A. M. 1992. Sequence of deformations recorded in joints and faults, Arches National Park, Utah. *J. Struct. Geol.* **14**, 225–236.